## *TITLE PAGE*

Report Title: **Fundamental studies and development of III-N visible LEDs for high-power solid-state lighting applications**

| | |
|---|---|
| Type of Report: | Final |
| Reporting Period Start Date: | September 1 2008 |
| Reporting Period End Date: | February 29 2012 |
| Principal Author(s): | Russell D. Dupuis |
| Date Report was Issued: | June 2012 |
| DOE Award Number: | DE-FC26-08NT01580 |
| Name and Address of Submitting Organization: | Georgia Institute of Technology<br>Atlanta, Georgia 30332 |
| Name, phone number and fax number of preparer: | Russell D. Dupuis<br>404 385-6094 and 404 385-6096 (Fax) |

## *ABSTRACT*

The goal of this program is to understand in a fundamental way the impact of strain, defects, polarization, and Stokes loss in relation to unique device structures upon the internal quantum efficiency (IQE) and efficiency droop (ED) of III-nitride (III-N) light-emitting diodes (LEDs) and to employ this understanding in the design and growth of high-efficiency LEDs capable of highly-reliable, high-current, high-power operation. This knowledge will be the basis for our advanced device epitaxial designs that lead to improved device performance. The primary approach we will employ is to exploit new scientific and engineering knowledge generated through the application of a set of unique advanced growth and characterization tools to develop new concepts in strain-, polarization-, and carrier dynamics-engineered and low-defect materials and device designs having reduced dislocations and improved carrier collection followed by efficient photon generation. We studied the effects of crystalline defect, polarizations, hole transport, electron-spillover, electron blocking layer, underlying layer below the multiple-quantum-well active region, and developed high-efficiency and efficiency-droop-mitigated blue LEDs with a new LED epitaxial structures. We believe new LEDs developed in this program will make a breakthrough in the development of high-efficiency high-power visible III-N LEDs from violet to green spectral region.

## *TABLE OF CONTENTS*

## *LIST OF GRAPHICAL MATERIALS*

Figure 15: Analyzed optical spectra of activated *p-InGaN* films taken at (a) room temperature (300K) and (b) low temperature (4K) measured by CL.

Figure 16: Emission spectra of a ~470nm blue-cyan light emitter with InGaN strain-relieving layer, showing significantly reduced wavelength λ shift <4.5nm from I=5 mA to 80 mA.

Figure 17: Peak intensity and wavelength change with different growth and structural parameters of green LED active.

Figure 18: Cross sectional TEM image of green LED structure with InAlN EBL.

Figure 19: Light output vs. current (*L-I*) curve of green LEDs (a) without EBL, (b) with HT-InAlN EBL, and (c) with LT-InAlN EBL; inset shows electroluminescence spectra of green LEDs with LT-InAlN EBL.

Figure 20: Cross-section TEM of the active region of the (a) LT-EBL and (b) HT-EBL device structures.

Figure 21: Room-temperature CL spectra of the QW emission of the three films.

Figure 22: Bandgap energy vs. lattice constant of III-N semiconductor materials showing lattice matching of In0.18Al0.82N to GaN.

Figure 23: Electronic band diagram of III-N visible LEDs with an Al0.2Ga0.8N EBL and an In0.18Al0.82N EBL.

Figure 24: Light output vs. current (*L-I*) characteristics of LEDs without an EBL, with an Al0.2Ga0.8N EBL, and with an In0.18Al0.82N EBL.

Figure 25: Quantum efficiency vs. current density for the LEDs without an EBL, with an Al0.2Ga0.8N EBL, and with an In0.18Al0.82N EBL.

Figure 26: EL spectra of (a) LED A, (b) LED B, and (c) LED C as a function of injection current, and (d) normalized quantum efficiency of the LEDs A, B, and C. LEDs A, B, and C have *p-InxGa1-xN*:Mg layers with xIn = 1.5%, 2.5%, and 3.5%.

Figure 27: EL spectra of TW-LEDs employing a *p-In0.025Ga0.975N* layer with Si doping in a selected QWB. Inset shows the location of Si doping in a selected QB.

Figure 28: Electronic band diagram of blue LED epitaxial structures with In0.18Al0.82N EBLs with thicknesses of 5, 10, and 20 nm.

Figure 29: Light output vs. current (*L-I*) and selected (for EBL thickness of 0, 5, and 15 nm) corresponding QE vs. injection current density (inset) of the LEDs with In0.18Al0.82N EBLs with various thicknesses.

## *INTRODUCTION*

Solid-state lighting (SSL) technology based on semiconductor light-emitting diodes (LEDs) [1] has been replacing conventional lighting technology based on incandescent or fluorescent lamps in *signaling/indicator* applications. All high-brightness UV, blue, and green light-emitting diodes (LEDs) made today are manufactured from the InAlGaN system, while the yellow, orange and red LEDs are made from the InAlGaP system, as shown in Figure 1. For broader and critical impact on energy conservation, the development of high-quality efficient and affordable SSL devices for illumination application is under way. For SSL *illumination* applications, "white" light source is required based on LEDs and two approaches have been developed in LED-based SSL technology:[2] One is based on phosphor-converted LEDs (PC-LEDs) and the other is on the mixing of three-colored R, G, B LEDs (RGB-LEDs). For both approaches, group III-nitride (III-N)-based blue and green LEDs are used in applications for full-color display and back-lighting and color-mixing-based general illumination lighting systems.[3] High-efficiency LEDs are projected to provide a dramatic reduction in the power necessary for industrial and commercial lighting and the full implementation of cost-effective high-performance SSL is projected by 2025 to reduce the electrical power used world-wide for lighting by over 50%.[4] Furthermore, the development of LED-based lighting products would, in the US alone, (1) save 1.66 Quads of electrical energy; (2) reduce the emission of carbon-containing atmospheric waste by 278M metric tons; and (3) generate a cumulative financial savings of $115B over the period 2000-2020.[4]

Significant challenges, however, remain to achieve the full potential of LED lighting, such as improvements in the peak internal quantum efficiency (IQE) and minimization of the efficiency decrease with increasing currents under high injection condition. The peak IQEs of blue and green LEDs are significantly lower than longer-wavelength InAlGaP-based red LEDs, especially for green LEDs, a feature referred to as a *green gap*.[5] In addition, the efficiency of blue and green LEDs based on III-N materials at high drive currents decreases with increasing injection current, often referred to as an *efficiency droop*.[6] These phenomena/problems were well-recognized, however, not completely understood. The green gap may be related to the quality of active region, resulted from highly-strained compromised-material-quality InGaN quantum wells (QWs) possibly accompanied by "random" phase separation.[7] The efficiency droop (ED) is even less understood, though recently published works have hinted at several (possibly inter-related and coupled) causes. It is clear that this is not a thermal issue but a fundamental problem associated with the InAlGaN materials and their heterostructures, unless the current density is extremely high under dc conditions (*e.g.*, $J$>350 A/cm$^2$) without proper thermal management.[8] Careful measurements of the LED junction temperature as a function of duty factor and current density reveal that this effect is purely dependent on current density.[9] Several suggested causes include high defect density combined with carrier delocalization from localized states in blue and green LEDs grown on *c*-plane sapphire substrates,[10-12] poor carrier injection into the InGaN quantum well active region induced by electron leakage due to band structure modification by polarization related to the growth of GaN on *c*-plane substrates,[13,14] poor carrier injection into lower QWs resulting in non-uniform carrier distributions between QWs induced by impeded hole transport,[15,16] and Auger recombination[17-19]. The relatively low IQE and substantial ED are considered to be ones of major technical challenges that need to be overcome for high-power high-efficiency LEDs for general illumination applications.

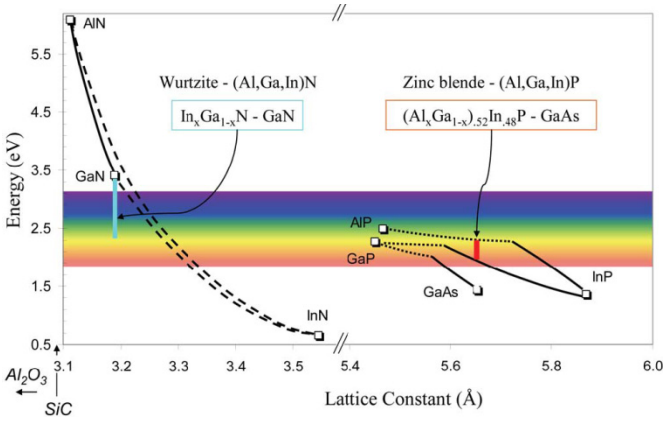


Figure 1: Bandgap energy vs. lattice constant of III-V semiconductor materials for visible light-emitting device applications.[20]

In this program, we will address the problems associated with low IQE and ED behavior in III-N-based epitaxial materials and structures. The goal of this program is to understand in a fundamental way on the impact of strain, defects, polarization, and Stokes loss in relation to unique device structures upon the IQE and ED of III-N LEDs and to employ this understanding in the design and growth of high-efficiency LEDs capable of highly-reliable, high-current, high-power operation. In this 36-month project, we have explored fundamental studies on materials and devices in combination with advance characterization techniques. We have also developed ED-mitigated and high-efficiency blue LEDs employing new epitaxial structures.

## *EXECUTIVE SUMMARY*

The goal of this program is to understand in a fundamental way the impact of strain, defects, polarization, and Stokes loss, and unique device active region designs upon the internal quantum efficiency (IQE) and efficiency droop (ED) of III-nitride (III-N) light-emitting diodes (LEDs) and to employ this understanding in the design and growth of high-efficiency high-power LEDs. This research includes three tasks: growth of high-quality III-N visible light emitter structures (Task 1); detailed characterization of III-N LED structures (Task 2) with subtasks of advanced material characterization of III-N LEDs (Subtask 2.1) and conventional material characterization for III-N MQW LEDs (Subtask 2.2); and design, processing, and testing of III-N LEDs (Task 3) with subtasks of LED device processing and testing (Subtask 3.1) and LED device processing and testing for high-power LEDs (Subtask 3.2). Much technical progress has been made for the achievement of the program milestones with focused studies on strain- and polarization-engineered LEDs.

The academic research in this program performed by Georgia Institute of Technology (PI: Russell Dupuis; co-PI: Jae-Hyun Ryou) and Arizona State University (co-PI: Fernando Ponce) was composed of activities in three main areas: materials growth using advanced metalorganic chemical vapor deposition systems; materials characterization using state-of-the-art electron microscopy, holography, and luminescence techniques; and device design, fabrication, and testing to develop visible LEDs with improved IQE and mitigated ED especially in the visible blue and green spectral region. We explored the control of LED epitaxial design factors that have limited the performance of III-N based visible LEDs. Under the supervise of P.I. and co-P.I.s, Dr. Hee Jin Kim (materials growth and characterization), Dr. Hyunsoo Kim (device fabriction and characterization), Mr. Suk Choi (materials growth and characterization), Mr. Jeomoh Kim (materials growth and characterization), Dr. Jiaping Liu (materials growth and characterization), Ms. Mi-Hee Ji (LED device fabrication and characterization), Mr. Zachary Lochner (materials growth and characterization), and Dr. Seong-Soo Kim (LED device fabriction and characterization) (Georgia Tech) and Dr. Alec Fischer (advanced materials characterization), Mr. Qiyuan Wei (advanced materials characterization), Mr. Ti Li (advanced materials characterization), Mr. Kewei Sun (advanced materials characterization), and Mr. Yu Huang (advanced materials characterization) (Arizona State Univeristy) cotributed to the research effort of this program.

For the study of the effects of crystalline defect and polarizations, we developed blue and green LEDs on *c*-plane and *a*-plane free-standing (FS) GaN substrates. For the LEDs on *c*-plane FS-GaN, in contrast to the substantial improvement in electrical and morphological properties, the emission intensity of the LEDs on the FS-GaN substrate is similar to that of the LEDs on the sapphire substrate. For the LEDs on *a*-plane FS-GaN, the absence of quantum-confine Stark effect is confirmed. These studies may, however, require further investigations, considering experimental uncertainties for fair comparison. For the study of hole transport and injection, we investigated effects of Si doping in quantum-well barrier (QWB), hole injection layers, and electron-blocking layers (EBLs). High Si doping in the QWB impedes the transport of hole and consequently causes non-uniform distribution of hole among QWs. In contrast, *p*-InGaN and tapered EBL enhance the hole transport, resulting in rather uniform hole distribution. For the study of effect of strain and polarization, we developed a new EBL scheme. InAlN EBL that is lattice-matched to GaN brings an improvement in quantum efficiency of green LEDs. In

addition, the InAlN EBL is more effective than a conventional $Al_{0.2}Ga_{0.8}N$ EBL in improving IQE and reducing ED. We also performed fundamental studies on the efficiency droop by both electron-spill over and limited hole injection, *p*-InGaN, and InGaN underlying layers.

Based on fundamental studies of the effects of various parameters in LED epitaxial structures, we demonstrated high-efficiency efficiency-droop-mitigated blue LEDs with a droop ratio of only ~4.5% at $J$~200A/cm$^2$.

## *EXPERIMENTAL*

### *1. MOCVD Growth of InAlGaN Heterostructures for LEDs*

The InAlGaN heterostructures used in this work were grown by metalorganic chemical vapor deposition (MOCVD) in a commercially manufactured and specially constructed Thomas Swan close-coupled showerhead (CCS) III-nitride reactor. The reactor system is designed to have a capability to accommodate up to seven 2-inch-diameter (or three 3-inch-diameter) wafers in one run. The substrates for the epitaxial structures of the LEDs and other related structures were *c*-plane (0001) sapphire or *c*-plane and *a*-plane (11-20) free-standing (FS) GaN substrates. Generally, non-indium (In)-containing III-N materials were grown in a $H_2$ ambient employing the primary precursors including trimethylgallium (TMGa, $(CH_3)_3Ga$), triethylgallium (TEGa, $(C_2H_5)_3Ga$), trimethylindium (TMIn, $(CH_3)_3In$), and trimethylaluminum (TMAl, $(CH_3)_3Al$) as alkyl sources, and ammonia ($NH_3$) as the hydride source. Silane ($SiH_4$) and bis(cyclopentadienyl)-magnesium ($Cp_2Mg$, $(C_5H_5)_2)Mg$) were employed as *n*-type and *p*-type dopant precursors, respectively. Layers containing In were typically grown in a $N_2$ ambient. For the growth of InGaN active layers, the growth temperature of 750~900 °C was employed. *In-situ* monitoring of the reflectivity of the wafer versus time and emissivity-corrected pyrometry by LayTec EpiTT system were employed to monitor growth temperature of the wafer, *in-situ* surface quality, and growth rate of the layers being grown.

### *2. Material Characterizations*

The properties of InAlGaN epitaxial heterostructures grown were investigated by a variety of material characterizations. The structural property of the epitaxial layers was characterized by X-ray diffraction (XRD) and transmission electron microscopy (TEM). XRD was employed to study crystalline qualities of GaN buffer and the layers subsequently grown from symmetric and asymmetric rocking curve scans. The line width of the peak on rocking curve scans closely related to mosaic spreading induced by various component of dislocations. XRD was also employed to study composition, thickness, and interface quality of multi-quantum well (MQW) active layers from triple-axis $\omega$-$2\theta$ scans in conjunction with simulation based on X-ray dynamical diffraction. Microscopic structural defects and features, such as total and each component dislocation density quantification, interface quality of MQWs, and possible defects induced by strain, InGaN layer, Mg dopant, etc.. The chemical properties of the layers were characterized by secondary ion mass spectrometry (SIMS) and Rutherford back scattering (RBS). SIMS was employed for dopant and impurity depth profiling. For accurate composition evaluation, RBS can be employed, since it does not require calibration of matrix materials. The optical properties of the structures were characterized by photoluminescence (PL), cathodoluminescence (CL), and time-resolved CL (TRCL). Especially, CL will be used to study the effect of phase separation on optical qualities of the MQWs. The electrical properties of the layers and structures were characterized by Hall measurement, *C-V* profiling, and contactless sheet resistance mapping system. Macroscopic and microscopic surface morphology of the layer is investigated by Nomarski optical microscope and atomic-force microscopy (AFM). Scanning electron microscope was employed to estimate the thickness and feature sizes of the hetero-epitaxial layers and device structures.

### *3. Device Fabrication Processing and Measurement of High-Power LEDs*

The fabrication process follows three important steps; namely, patterning etch mask, mesa isolation etch, and metallization processes. First, pattern by $SiO_2$ etch mask using conventional lithography and liftoff, followed by mesa isolation with a $SiO_2$ etch mask using inductively-coupled plasma reactive-ion etching (ICP-RIE) was performed. The $SiO_2$ mask exhibits good selectivity (~10:1) over the layer to be etched, when etching GaN. Once the mesa was defined, metallization step followed, by depositing bottom layer (*n*-GaN) ohmic contact which is typically Ti/Al/Ti/Au. As the last step, *p*-GaN layer ohmic contacts which can be Ni/Au (semi-transparent) or Ni/Ag/Pt (reflective) metallization were deposited. All metallization processes were done by E-beam evaporation. Contact annealing was performed at 500 °C for 1 minute. Once fabrication was done, we first characterized the electrical performance using semiconductor parameter analyzer. The quality of ohmic contacts was studied by TLM (transfer line method) characterization. Diode *I-V* characteristics were also measured. Electroluminescence (EL) performance characteristics were measured either by a "quick" LED test set up on an epitaxial wafer by using indium dot contacts or by "full" LED testing on processed LEDs on the chip level without packaging.

## *RESULTS AND DISCUSSION*

The goal of this program is to understand in a fundamental way on the impact of strain, defects, polarization, Stokes loss, and unique device active region designs upon the IQE and ED of III-N LEDs and to employ this understanding in the design and growth of high-efficiency, high-power, and droop-mitigated visible LEDs for next-generation SSL for general illumination applications. This research includes three tasks: growth of high-quality III-N emitter structures by MOCVD (Task 1); detailed materials characterization of III-N light-emitting diode structures (Task 2) with subtasks of advanced microstructural material characterization of III-N LED structures (Subtask 2.1) and macroscopic conventional material characterization for III-N LED epitaxial structures (Subtask 2.2); and design, processing, and testing of III-N LEDs (Task 3) with subtasks of LED device processing and testing (Subtask 3.1) and LED device processing and testing for high-power LEDs (Subtask 3.2). Our research activities for the phases I, II, and III of this program are summarized as follows:

### *1. Green LEDs grown on c-plane sapphire and free-standing GaN substrates*

*This study includes tasks 1, 2.2, and 3.2 with a focus on the effect of defects on the IQE of III-N LEDs with long-wavelength emission.*

Green LED structures using InGaN:Mg as the hole injection and contact layers were grown on *c*-plane (0001) FS-GaN substrates and sapphire substrates. Since the nano-pits that were shown on the surface of the green LEDs with *p*-InGaN:Mg, which have been developed for active-region-friendly and quantum-confined-Stark-effect (QCSE)-controlled LEDs[21-24] under the previous DoE SSL program (DoE DE-FC26-03NT41946), are known to originate from the threading dislocations, it is expected that the density of the pits is reduced as the threading dislocation density decreases. Also, there have been several reports on the characteristics of LEDs grown on FS-GaN substrates; however, their operating wavelengths were focused on violet and blue spectral region and the LEDs showed different (and often contradictory) characteristic performances. Since the In segregation in the InGaN QW was reported to be affected by the dislocation and the phase separation behavior was reported to be different in green InGaN MQW active region with high In content, optical characteristics and structural and electrical properties of the green LEDs grown on FS-GaN substrates with reduced dislocation densities can be different. In addition, this study can be extended to the effect of defect density in the epitaxial structures on the luminescence efficiency (mainly IQE) and ED of the visible LEDs.

The pit density of LEDs grown on a FS-GaN substrate is ~2 orders of magnitude lower than that of LEDs grown on a sapphire substrate, which agrees with the fact that the dislocation density of the FS-GaN substrates (the order of $10^6$ $cm^{-2}$) is ~2 orders of magnitude lower than that of GaN templates grown on sapphire substrates (the order of $10^8$ $cm^{-2}$), as shown in AFM images of Figure 2. As a result, the reverse current at -10 V of the LEDs grown on the FS-GaN substrate (the order of $10^{-9}$ A) is ~2 orders of magnitude lower than that of the LEDs grown on the sapphire substrate (the order of $10^{-7}$ A), as shown in Figure 3. However, in contrast to the improved electrical and morphological characteristics, the emission characteristics of the LEDs grown on the FS-GaN substrate are similar (or only slightly improved, in not same) to those of the LEDs grown on the sapphire substrate, as shown in Figure 4, even though the line-width of the EL peak becomes slightly narrower, with a full-width at half maximum (FWHM) of 30 nm

for the LED on the FS-GaN substrate versus 33.8 nm for the LED on the sapphire substrate. The results and further discussion were reported in detail in ref. 25.

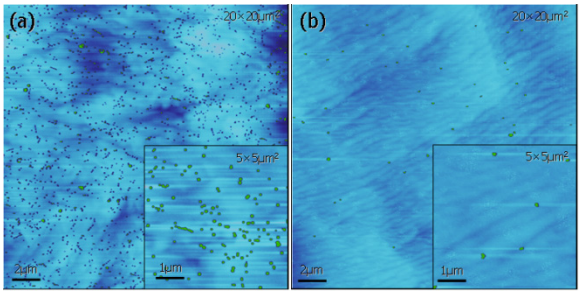


Figure 2: AFM microscopic surface morphology of the green LED epitaxial structures grown on (a) a sapphire substrate and (b) a FS-GaN substrate. The scan area is 20×20 μm$^2$ and the inset image scan area is 5×5 μm$^2$.

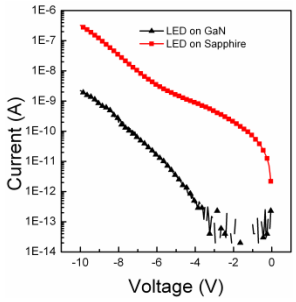


Figure 3: Reverse current-voltage curves for LEDs.

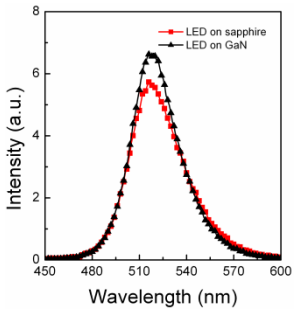


Figure 4: EL spectra of green LEDs at a current of 20 mA.

This study on the effect of crystalline defect (mainly line defects, not necessarily point defects and others), especially on the ED as well as IQE, may require further investigations. For the comparison of visible LEDs on sapphire substrates and FS-GaN substrates, experimental results among the research groups are not consistent and the effect of threading dislocation on the performance characteristics, especially on luminous characteristics, is still inconclusive. Liu, *et al.* and Cao, *et al.* reported comparable light output for the LEDs on both substrates at low current densities, while the FS-GaN-based LEDs exhibited improved electrical characteristics including leakage current and materials quality.[25,26] In contrast, Kyono, *et al.* reported improved light output for the LEDs on GaN substrates.[27] These observed inconsistencies may arise from inaccurate comparisons. First, light-extraction efficiencies are different for the LEDs on sapphire and FS-GaN substrates mainly due to different refractive indices of the substrates. Also, even with nominally the same growth conditions for the LEDs on both substrates, actual growth condition on the growing surface may be different mainly due to significantly different thermal conductivities of those substrates. We have calculated temperatures of the growing surfaces depending on the substrates (*e.g.*, sapphire, GaN, AlN, SiC, and Si) at various temperatures under various hydrodynamic conditions.[28] The results showed that the actual temperature of the growing surface can differ by >5 °C on sapphire and GaN substrates under a typical InGaN growth condition for long-wavelength green QWs in CCS-MOCVD reactors, *i.e.*, a nominal growth temperature of ~780 °C with a convention heat transfer coefficient *h* of ~225. This difference can make a significant change in the In composition and crystalline qualities, including point defects such as impurities. Besides actual growth temperature, the density and nature of the threading dislocations may affect the formation of localized states in InGaN QWs,[29,30] which is believed to affect the IQE. Finally, probably the most critical but not very well-known effect is the uniformity effect of FS-GaN on luminescence properties. While luminescence uniformity of the LEDs on the sapphire substrates depends on temperature and precursor flux density, which can be controlled in well-designed reactor chambers, the uniformity of the FS-GaN substrates is more dependent on the "uncontrolled" tilt-angle variation of the substrates in addition to the growth chamber uniformity. The FS-GaN substrates are

prepared from a thick epitaxial film grown on foreign substrates that inherently have a large bowing in the film during the growth and subsequent cool-down. Slicing and polishing with a straight parallel direction for a FS-GaN substrate result in large tilt-angle variation depending on the location of the area being measured on the substrates. We have experiences with the development of visible laser diodes (LDs) on 2-inch FS-GaN and have confirmed that only small portion of LEDs/LDs from a certain area on 2-inch FS-GaN with a proper orientation showed bright optimized luminescence, hence better performance characteristics, from wafer uniformity studies, which suggest that random selection of the LEDs on FS-GaN may result in erroneous experimental results/conclusion in comparison studies. In order to avoid this possibility and take advantage of further improved crystalline qualities, we may want to use "true-bulk" GaN substrates (bulk-GaN)[i] for further studies. As described, a fair comparison for the effect of threading dislocation on luminescence properties has shown limitations to date. The situation is even worse for the effect on ED due to the more complicated nature of experimental conditions require for the study of the droop. For example, the ED behavior has been improved for some LED structures on FS-GaN over sapphire substrates, while it has not been improved for other LED structures on FS-GaN even in the same report.[31] Furthermore, it is well known that the dislocation density is important in the performance and reliability of III-N LDs and since high-power LEDs operate in the same current density and junction temperature range, the performance and reliability of power LEDs could be impacted by these same factors.

In summary, we investigated the effect of threading dislocations on the IQE of green LEDs employing *p*-InGaN:Mg on a FS-GaN substrate. In contrast to the substantial improvement in electrical and morphological properties, the emission intensity of the LEDs on the FS-GaN substrate is similar to that of the LEDs on the sapphire substrate. This study will require further investigations, considering experimental uncertainties for fair comparison.

### *2. Visible LEDs on a-plane free-standing GaN substrates*

*This study includes tasks 1, 2, and 3.2 with a focus on the effect of polarization on the IQE of III-N LEDs with long-wavelength emission.*

We grew the green LED structure on a non-polar (11-20) *a*-plane FS-GaN substrate. The surface morphology of GaN homoepitaxial layer on non-polar substrate is often reported to have rough and anisotropic textured surfaces. Our optimized GaN homoepitaxial growth condition produced smooth surface without textures under Nomarski optical microscope (data now shown here). The RMS surface roughness of AFM images of as-received substrate and GaN homoepitaxial layer are 0.35 and 0.128 nm for $1\times1$ $\mu m^2$ scan, suggesting that surface recovering can occur by grown GaN layer under optimized condition.

Green LED structure was grown on a non-polar *a*-plane FS-GaN substrate using the same epitaxial structures as described in the section 1 of the results and discussion, which is 5-period MQW InGaN/GaN active region with *p*-InGaN hole injection and contact layers, and nominally same growth condition. We can expect the wavelength will be changed for LEDs on non-polar substrate due to the absence of internal field in the QW, different growth chemistry, etc..

Figure 5 shows surface morphology of the LED structures grown on a non-polar *a*-plane FS-GaN substrate. Microscopic morphology measured by AFM shows slight roughening but we think the surface is still decent and much better than other non-polar surfaces (Figure 5 (a)). The

[i] True "bulk GaN" substrates from bulk GaN crystals grown using an ammono-thermal process, have been commercially developed by Ammono Sp. in Poland and are currently available up to 1.5 inch diameter.

RMS roughness is 0.55 nm for the green LED epitaxial structures for 5×5 μm$^2$ scan. Under Nomarski, the surface shows specular surface under high magnification (Figure 5 (b)), but trapezoidal pits and texturing, which was not shown in optimized GaN homoepitaxial layer, is observed under low magnification (Figure 5 (c)).

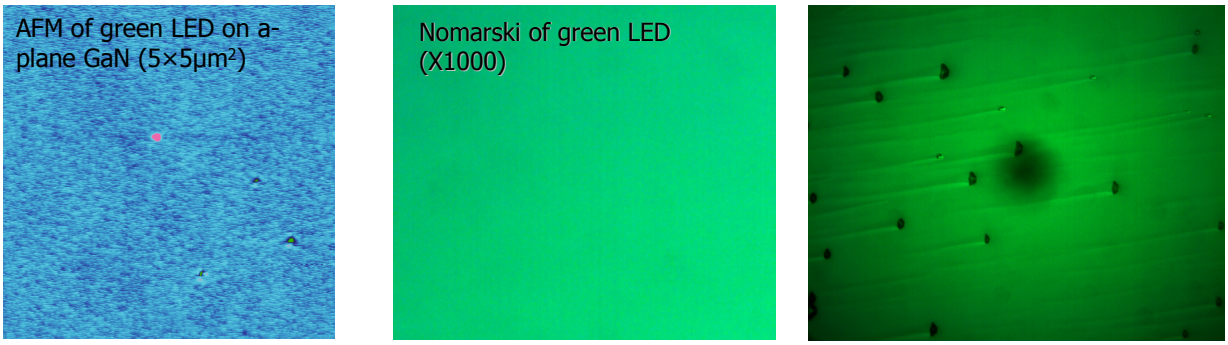


(a) (b) (c)

Figure 5: Surface morphology of the LED structures grown on a non-polar *a*-plane FS-GaN substrate: (a) AFM (5×5 μm$^2$), (b) Nomarski optical microscopy (×1000), and (c) Nomarski optical microscopy (×500).

Figure 6 shows the optical properties of visible LED structures grown on a (11-20) *a*-plane GaN bulk substrate. We ended up with blue emission of visible LEDs on non-polar substrate at λ~450 nm. PL peak from the QW is not very bright as compared to that from *p*-InGaN (at 376 nm) and weak defect-related peak corresponding to red visible spectrum is also observed. Current-dependent EL does not show any of blue shift of peak wavelength with current. Instead, peak remains until *I*~50 mA and then begin red shift with increasing current. This is due to absence of the QCSE (low current up to *I*<~50 mA) and heating effect (high current *I*>~50 mA). The peak intensity itself is, in general, lower than that of other blue LEDs grown on *c*-plane substrates.

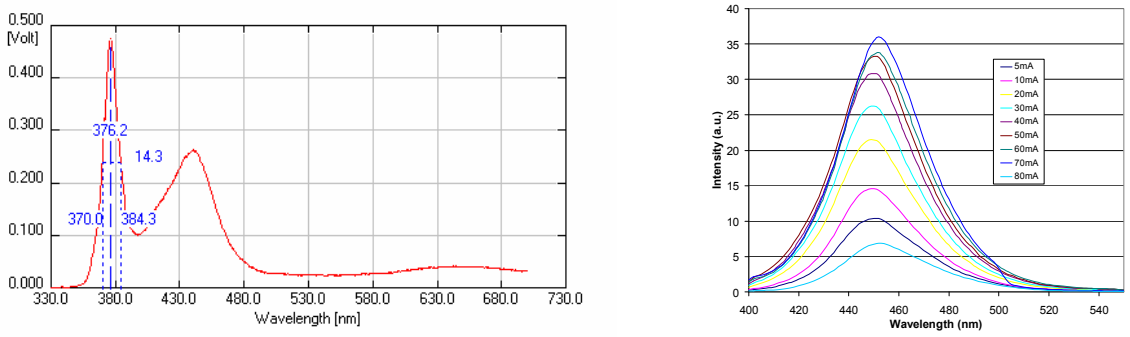


(a) (b)

Figure 6: (a) PL of a LED epitaxial structure and (b) current-dependent EL from fabricated LED devices grown on a (11-20) *a*-plane FS-GaN substrate.

Series resistance of the diode is ~40 Ω which is higher than that of counterpart on polar substrate by the factor of two magnitudes (data not shown here). This suggests that we may need further optimization to improve electrical and optical characteristics. Microscopic structural analysis was done by TEM. We expected several structural defects such as stacking faults;

however, surprisingly we have not observed any of stacking faults. Figure 7 shows TEM image of active region with different conditions showing, stacking-fault-free materials. 5-period MQW is clearly shown and the interface quality looks decent. Figure 8 shows luminescence from fabricated LED devices grown on a (11-20) *a*-plane FS-GaN substrate, showing blue emission. When low current is injected, preferred emission of light near the pit region is observed. This may be related to many possibilities: more efficient photon generation near pits; more efficient light extraction near pits; preferable current injection near pits.

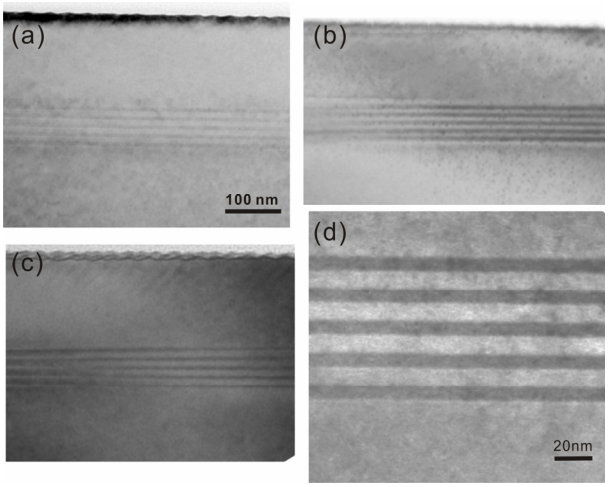


Figure 7: TEM of active region of LED structure grown on a (11-20) *a*-plane FS-GaN substrate.

(a) (b)

Figure 8: (a) Bird's eye view of light emission and (b) picture of light output (at low current level) from fabricated LED devices grown on a (11-20) *a*-plane FS-GaN substrate.

The results and further discussion were reported in detail in ref. 32.

In summary, we investigated the effect of polarization and QCSE on the IQE of visible LEDs employing a (11-20) *a*-plane FS-GaN substrate. The EL spectra of the LEDs at the peak wavelength of λ~450 nm are independent of current level at low current densities before the heating effects are evidenced, that confirms the absence of the QCSE. However, the electrical, morphological, and luminous characteristics of the non-polar *a*-plane LEDs will require further improvement.

### *3. Effect of Si-doping in the quantum well barrier (QWB) of III-N LEDs*

*This study includes tasks 1, 2, and 3.2 with a focus on the effect of hole transport on the IQE of III-N LEDs with long-wavelength emission.*

Effects of Si doping have been discussed from various points of view (improved surface morphology of GaN QWB by Si doping grown at lower temperatures, screening of QCSE by Si doping, improvement in the interface qualities by Si doping, stronger localization effects and higher mobility by light Si doping, blocking effect of hole transport by Si doping, etc.) and many LEDs and LDs employ a certain level of Si doping (usually lightly-doped) in the QW and/or QW barrier (QWB); however the effects of doping on device performance characteristics are still somewhat unclear and sometimes controversial. We investigated the effect of Si doping in the QWB of the green LED structures on the optical and electrical characteristics. The Si dopant precursor flow rate was changed from 0 sccm (standard cubic centimeter per minute) to 8 sccm, which corresponds to a molar flow rate of ~$3.6\times10^{-3}$ μmol/min ($SiH_4$=10 ppm concentration balanced in $H_2$). Donor concentrations, $N_D$, for 1 sccm, 4 sccm, and 8 sccm of dopant precursor flow rate are estimated to be $5\times10^{17}$ $cm^{-3}$, $2\times10^{18}$ $cm^{-3}$, and $4\times10^{18}$ $cm^{-3}$, respectively. As the Si doping level increases from 0 sccm, the peak intensity of EL decreases almost linearly, as shown in Figure 9. XRD and AFM were used to investigate the effect of Si doping on material quality of QWBs and interface quality of QW/QWB active regions. We do not observe differences in peak intensities and line widths of superlattice-related peaks in XRD ω-2θ scans between LEDs with various levels of Si doping in the QWBs. In addition, the growth mode transition from spiral growth to layer-by-layer growth is not observed for LEDs having QWBs with Si doping. The microscopic morphology of the QWBs, measured by AFM, shows atomically smooth surface regardless of doping level of Si in QWB. A significant peak wavelength shift depending on the Si doping in the QWBs is not observed for LEDs. either. Figure 10 (a) shows the EL spectra of the fabricated LEDs with undoped QWBs and Figure 10 (b) shows EL spectra of the LEDs with QWBs heavily-doped with Si. Peak wavelengths at a current of $I$=30 mA ($J$~25 A/$cm^2$) and $I$=70 mA ($J$~57 A/$cm^2$) for fabricated LEDs with undoped QWBs are ~499 nm and ~497 nm, respectively. For the LEDs with QWBs doped with Si=4 sccm, the peak wavelengths are ~501 nm and 499 nm at $I$=30 mA and $I$=70 mA, respectively. Therefore, we believe Si doping does not significantly change the material and interface quality of the active region in our growth condition. This suggests that Si doping should not affect the material quality, as also evidenced by the XRD and AFM results. Instead, Si doping in the QWBs may dominantly affect the hole transport by altering the potential barrier height of the QWBs. With increasing Si doping in the QWBs, the potential barrier height of QWBs for hole transport becomes higher, while the QWBs height for electron transport becomes lower. Therefore, it becomes difficult for hole transport to occur into the lower QWs (close to the *n*-GaN layer). This hole transport blocking effect by Si doping in the QWB may cause inhomogeneous hole distribution between QWs, that is, more holes in QWs near the *p*-type layer and fewer holes in QWs near the n-GaN layer. The result is a lack of holes available for radiative recombination in the QWs located close to the *n*-GaN layer, which makes the luminescence of the LED less efficient. This hole transport blocking effect and resulting inhomogeneous hole distribution between QWs is believed to be more significant in longer-wavelength LEDs with high-In-content InGaN QWs having higher potential barriers between QWs and QWBs.

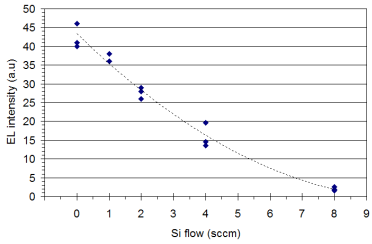


Figure 9: EL peak intensities of the LED structure with various Si doping in the QWBs measured by wafer-level quick test.

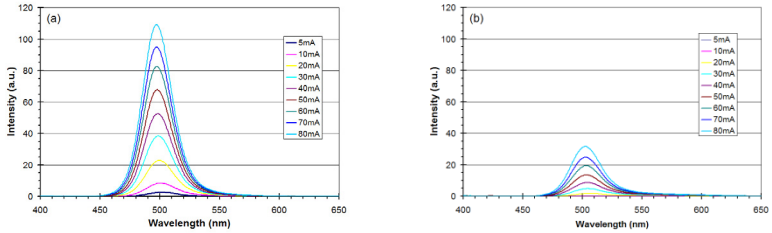


Figure 10: EL spectra of the LEDs with various Si doping in QWBs measured from fabricated devices: (a) undoped QWBs (Si=0 sccm) and (b) QWBs doped with Si=8 sccm.

The electrical properties of LEDs are also characterized from fabricated devices. Figure 11 shows *I-V* characteristics of LEDs. As the Si doping in the QWBs increases, the turn-on voltage decreases. Forward voltages at 20 mA are 3.85, 3.65, and 3.48 V for Si= 0, 4, and 8 sccm. As the Si doping increases, the electron diffusion current can be enhanced, and this makes the forward voltage at low current levels decrease. After turn-on, however, the series resistance is similar at ~28 Ω in the range of V=3.5~4 V. In summary, for the improvement of internal quantum efficiency and wall-plug efficiency of the LEDs, the effects of Si must be carefully considered in the design and growth of visible LEDs, especially for green LEDs with relatively long operating wavelengths. The results and further discussion were reported in detail in ref. 33.

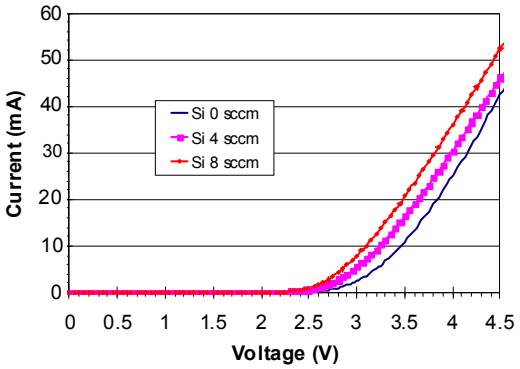


Figure 11: Forward-bias *I-V* characteristics of the LEDs with various Si doping in QWBs.

In summary, we investigated the effect of Si doping in the QWB on the IQE of green LEDs with a focus on carrier dynamics. As the Si doping concentration in the QWBs increases, the EL peak intensity decreases and the turn-on voltage decreases, which is believed to be mainly due to electron transport enhancement and the hole transport blocking effect. For the improvement of IQE and wall-plug efficiency of the LEDs, the effects of Si must be carefully considered in the design and growth of visible LEDs, especially for green LEDs with relatively long operating wavelengths.

### *4. Effect of hole transport and resulting carrier distribution in MQWs of III-N LEDs*

*This study includes task 3.2 with a focus on the effect of hole transport on the IQE and ED of III-N LEDs.*

We have suggested that non-uniform carrier distributions governed by impeded hole transport in InGaN/GaN multiple quantum well (MQW) active region in visible LEDs is related to the ED.[15] This problem exists in all commercially available blue and green LEDs. This reduced efficiency is accompanied by a blue-shift of the operating dominant wavelength as the current density increases, and the magnitude of the problem increase as the emitting wavelength of the LED moves to longer wavelengths. Among many possible origins of ED, as we suggested, we focused on electron and hole transport and resulting in non-uniform carrier

distributions among the MQWs. In collaboration with Prof. Yoder's group at Georgia Tech, we have studied the carrier distribution in the InGaN MQW active region of visible light emitters – in this specific case, it is a typical InGaN/GaN three-period MQW active region and waveguide structure with an AlGaN electron blocking layer (EBL). Figure 12 shows the electron and hole densities in the MQWs, revealing non-uniform carrier distributions. It shows several salient features of typical III-nitride-based light emitter active regions: (1) it shows spatial separation of electron and hole peak densities, as expected from polarization-induced QCSE in the QWs; (2) at a position of approximately 1644 nm, a local, unintentional suppression of the energy of the conduction band edge is evident, and its influence is reflected in the electron charge density. This is significant for InGaN-based light emitters for two reasons: (1) it represents a substantial fraction of the injected electrons which, although prohibited from passing into the *p*-type layers above by the EBL, may not contribute to optical gain and these carriers are subject to non-radiative recombination. It is important to note that the electron density in the parasitic inversion layer is comparable to that in the three adjacent well regions, meaning wasting substantial number of electrons not to be used for radiative recombination; (2) it is also clear from Figure 12 that the hole density is far from uniform across the three QWs. As discussed above, a unifrom distribution of carriers between QWs and confinement in the QW (not in potential minima by the EBL) to be used for efficienct radiative recombination are of critical importance. The engineering of carrier distributions is keenly noticed to be a key technology to improve the peak efficiency of the IQE and to mitigate the ED problem. This requires strain and polarization engineering as well as electronic band structure engieering in active region of the LEDs.

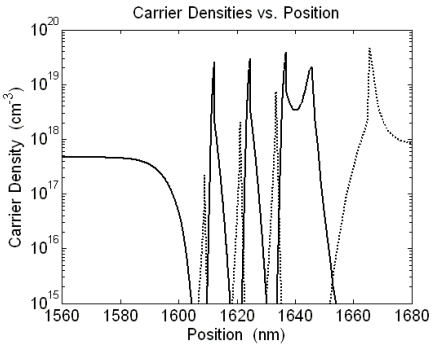


Figure 12: Simulated electron (solid curve) and hole (dotted curve) densities reveal non-uniform hole distribution among QWs in a typical InGaN/GaN MQW with AlGaN EBL structure. Applied bias is 3.6V

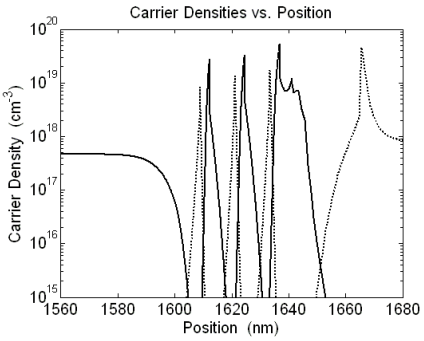


Figure 13: Simulated electron (solid curve) and hole (dotted curve) densities reveal improved uniformity in hole distribution among MQWs using the tapered design strategy. Applied bias is 3.6 V.

With this understanding of the origin of the non-uniform hole distribution among MQWs, we propose two strategies for ameliorating the deleterious influence of the parasitic inversion layer. First, by tapering the transition between the barrier and the EBL material, it is possible to spatially distribute the piezoelectric polarization charge of the original interface, and in so doing reduce or eliminate the parasitic inversion layer altogether. Secondly, *p*-type doping of the upper half of the transition region may help lower the electron chemical potential with respect to the conduction band edge, while inflicting minimal penalty to crystal quality in the active region. To demonstrate the efficacy of this approach, we replace the 8nm thick barrier material above the top well with one 4-nm layer of $Al_{0.04}Ga_{0.96}N$ followed by two 2-nm layers of $Al_{0.09}Ga_{0.91}N$ and

$Al_{0.14}Ga_{0.86}N$. These top two layers are assumed to contain an active Mg concentration of $1\times10^{18}$ $cm^{-3}$. As Figure 13 demonstrates, the tapered design strategy affects a significant improvement in the uniformity of bound holes among the MQWs. Optimized tapered designs are anticipated to afford yet further improvement. Finally, we note that the tapered design strategy will necessarily perturb the optical characteristics of the top well, but this may be easily corrected with a minor redesign. Further optimization of design for further improvement of hole stransport and uniform distribution is planned. The results and further discussion were reported in detail in ref. 34.

### *5. Microstructural study of p-InGaN layers*

*This study includes tasks 1 and 2.1 with a focus on fundamental nature of p-type InGaN layer that can be used for hole injection layers in visible LEDs.*

Several *p*-type $In_xGa_{1-x}N$:Mg samples with various In compositions and electrical properties (sample # 2-0989-2, 2-0994-2, 2-0996-2, 2-0997-2, and 2-0998-2) were characterized by ASU group for microstructural and optical characterizations of the materials. This study is the part of following approaches to (1) understand the limitation of growth of high indium content InGaN thick layers; (2) to study mechanisms of lattice misfit relaxation in wurtzite structures; and (3) to study magnesium doping of InGaN and the capability to produce *p*-type layers. Table 1 shows the detailed description of the samples including compositions, bandgap energies, and their electrical properties. Both as-grown (Mg dopant unactivated) and $N_2$ annealed (Mg dopant activated) samples were provided for the sample grown in the same growth condition. Figure 14 shows the results of analyzed CL optical spectra of unactivated *p*-InGaN films taken at 300K and 4K. At room temperature (300K), a red-shift of InGaN-related donor-bond exciton (D°X) with increasing indium composition was observed due to shrinkage of the band gap. The relative shift between the D°X energy position and the bang gap energy were constant, but the relative shift decreases for higher indium compositions. The red-shift of InGaN-related donor-acceptor pair (DAP) was observed with increasing In composition. The relative shift is somewhat constant. At low temperature (4K), we observed the e-A transition, and a red shift of the transition with the bandgap energy. A red-shift of InGaN-related DAP with increasing indium content was observed. The relative shift of these transitions with the band gap becomes smaller in the sample for $x_{In}$~0.04, suggesting that their respective acceptor activation energies reduce with decreasing bandgap energy. In addition, a new transition was observed for e-dose = $8.06\times10^{16}$ e/sec/$cm^2$. The peak wavelength of this transition red-shifted with decreasing bandgap energy, and the relative shift of both was constant.

Table 1: In composition, bandgap energies, and electrical properties of *p*-type $In_xGa_{1-x}N$ samples for microstructural and optical characterizations.

| Sample | Indium molar content | Band gap | Band gap | Bulk resistivity | Mobility |
|---|---|---|---|---|---|
| | | eV | eV | ohm-cm | cm^2/V-s |
| | | RT | LT | Bulk resistivity | Mobility |
| | | b=1.43 | b=1.43 | | |
| 2-0989-2 | 0.014 | 3.37824 | 3.44402 | 1.32 | 7.43 |
| 2-0994-2 | 0.0177 | 3.36281 | 3.42852 | 1.2 | 7.62 |
| 2-0996-2 | 0.0279 | 3.32046 | 3.38601 | 0.846 | 8.59 |
| 2-0997-2 | 0.036 | 3.28704 | 3.35247 | 0.719 | 13.8 |
| 2-0998-2 | 0.0424 | 3.26077 | 3.32609 | 0.539 | 7.44 |

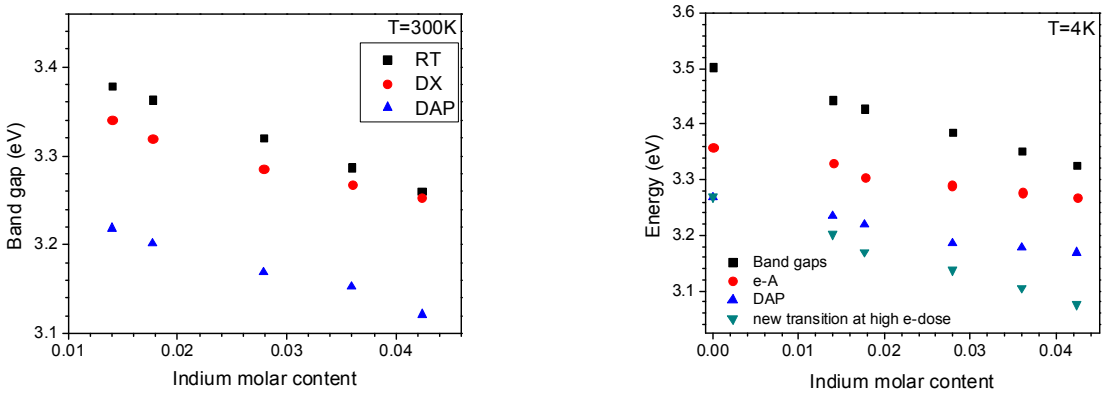


Figure 14: Analyzed optical spectra of unactivated *p*-InGaN films taken at (a) room temperature (300K) and (b) low temperature (4K) measured by CL.

Figure 15 shows the results of analyzed CL optical spectra of activated *p*-InGaN films. Similar trends of lines were observed such as a red-shift of InGaN-related D°X and DAP with increasing indium composition due to shrinkage of the band gap, decreasing relative shift with the bandgap energy with increasing In composition, and no change in spectrum with increasing electron-dose. At low temperature, we observed the e-A transition, and a red-shift with the bandgap energy. The InGaN-related DAP red-shifted with increasing indium content. The relative shift of these transitions with the band gap was constant. Also, an acceptor mini-band could be responsible of this effect, since these transitions are expected to have different relative shifts. The relative shift of the InGaN-related DAP did not change with increase of electron-dose. Activated films did not change their luminescent properties with increase of electron-dose.

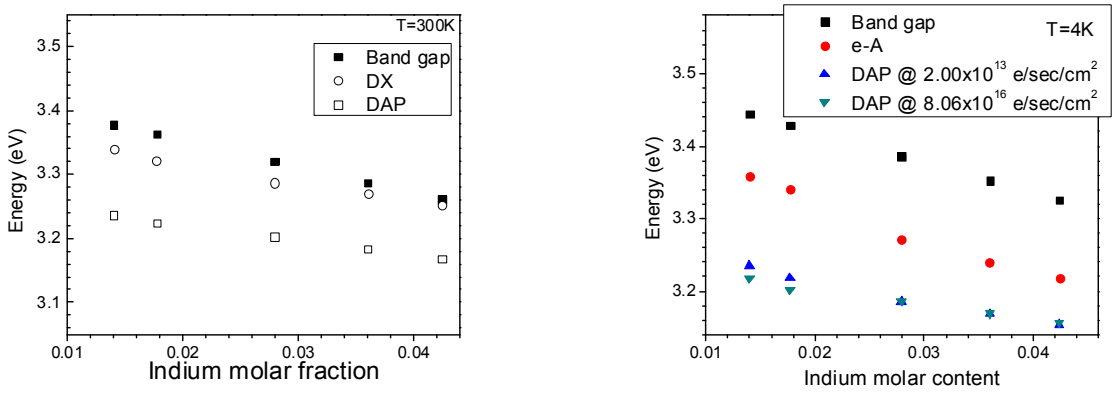


Figure 15: Analyzed optical spectra of activated *p*-InGaN films taken at (a) room temperature (300K) and (b) low temperature (4K) measured by CL.

## *6. Strain- and QCSE- controlled active region development and EH characterization of strain-engineered LED active region*

*This study includes tasks 1 and 2.1 with a focus on the effect of strain and QCSE in MQW by strain modification in visible LEDs.*

The QCSE in combination with the polarization effect is believed to be one of major factors that limit the IQE and that cause ED of LEDs. Especially for long-wavelength green LEDs, these effects expected to be more significant. In $In_xGa_{1-x}N$ MQW active region for visible LEDs, the polarization effect is significantly induced by piezoelectric polarization effect in the QW, which is induced from a strain built in the QW. In order to mitigate the strain in the QW, that is, the QCSE-mitigated LEDs, we have developed LED structures with a modified strain in the *p*-type layer.[21] In order to further improve our QCSE-controlled LED structure, we are developing the LED structures with a modified strain near the QW active region. The modified strain effect of the layer located closer to the QW is expected to be more significant. One of the possible strategies is employing a "strain-relieving" InGaN layer near (top and bottom of) the active region. In order for the strain-relieving layer to be effective, the layers need to be reasonably thick and the material quality should not be compromised. Especially, the InGaN layer is reported to have V-defects when the In composition is high and/or the layer is thick enough. The study of the materials quality and the thickness of strain-relieving InGaN layers was extensively carried out in terms of surface morphology and quick-test EL. The surface morphologies were studied to find the optimum growth condition for the material qualities especially for V-defect-free surfaces. Also, quick-test EL was employed to find the optimum thickness and composition of strain-relieving InGaN layer. Figure 16 shows the quick test EL spectra of one of optimized active region structure with InGaN strain-relieving layer, showing significantly reduced wavelength shift of <4.5nm with increasing current injection from *I*=5 mA to 80 mA. In order to further investigate the effect of InGaN strain-relieving layer on the QCSE, four samples were grown with different strain-relieving layer structures and different emission wavelengths and delivered to ASU Ponce group for the measurement of electrostatic potential in the QWs by electron holography technique. They included the LEDs structures with emission wavelengths of 420nm (violet) and 470nm (blue-cyan) for different built-in strain in the QW (hence, different QCSE) and with InGaN and GaN strain relieving layers for different strain-relieving effect on the QW active region. In order to further investigate the effect, four samples were grown with different strain-relieving layer structures and different emission wavelengths and delivered to ASU group for the measurement of electrostatic potential in the QWs by EH technique. Two of them were characterized and compared: 2-1567 with 80nm $In_{0.03}GaN$ layer and 2-1568 with 100nm n-GaN layer underneath the same InGaN/GaN MQW active region. As shown in Figure 17, for sample 2-1567, the suppression of internal field in the 1st QW right upon the InGaN layer was clearly observed, while for sample #1568 the internal field is uniform and ~0.75 MV/cm across each quantum well. The 80nm $In_{0.03}GaN$ layer might be not sufficiently thick to be fully relaxed. However, the strain in the 1st quantum

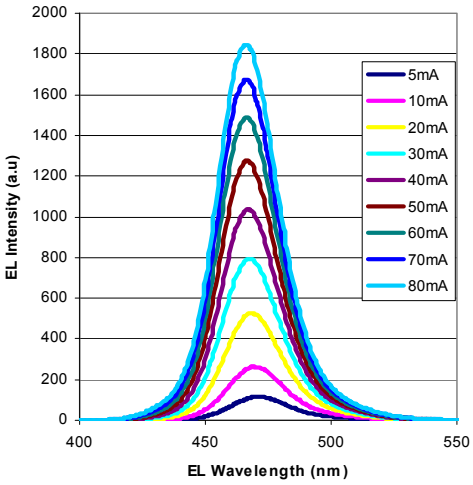


Figure 16: Emission spectra of a ~470nm blue-cyan light emitter with InGaN strain-relieving layer, showing significantly reduced wavelength λ shift <4.5nm from I=5 mA to 80 mA.

well has been significantly reduced. This may suggest we need further strain engineering near the QW region to be effective for all the QWs. In addition, this strain-relieving layer may affect the In incorporation of the QWs by an effect called "composition pulling". A small amount of indium and the lower growth temperature for the underlying layer could affect the QW growth dramatically.

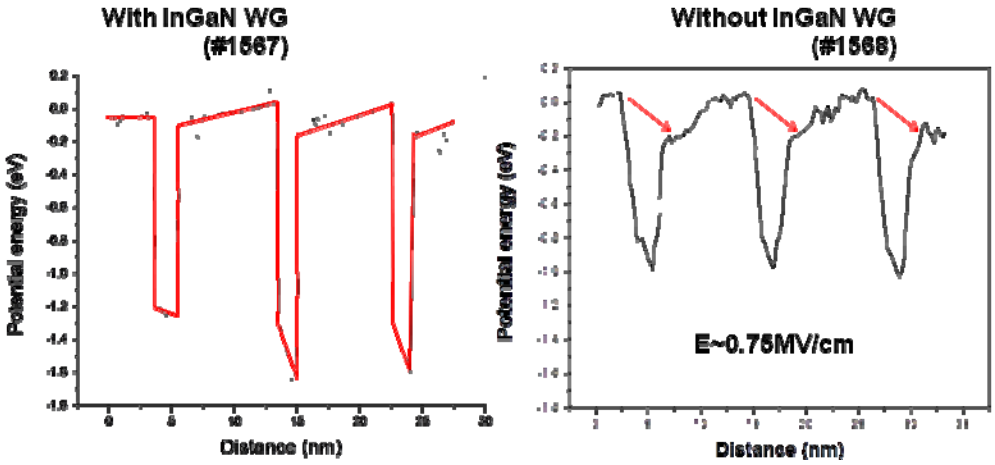


Figure 17: Peak intensity and wavelength change with different growth and structural parameters of green LED active.

### *7. Strain-, polarization-, and electronic band-structure-engineered green LED active region with an InAlN electron blocking layer*

*This study includes tasks 1, 2, and 3.1 with a focus on the effect of electron spill-over on the IQE in green LEDs.*

We have also developed new EBL structure with an active-region-friendly and lattice-matched InAlN layer. This new EBL was employed in the green LED structure, as shown in Figure 18. The InAlN EBL is expected to provide a more effective electron confinement (than typical AlGaN EBLs) without detrimental effects due to lattice mismatch and high growth temperatures (which is generally accompanied by AlGaN EBL growth). The effect of the InAlN EBL on the luminous characteristics was studied by EL measurements performed under DC-bias conditions. The injection current ($I$) was varied up to 80 mA (equivalent to $J$=65.3 A/cm$^2$) and all the LEDs with and without InAlN EBLs show similar line-widths and peak wavelengths in the EL spectra, *e.g.*, peak wavelength at λ~530 nm at $I$=50 mA (data not shown except the EL spectra of an LED with a LT-InAlN as in the inset of Figure 19). Figure 19 shows the variation of the integrated EL intensity with injection current density. All the LEDs show similar full-width at half-maximum (FWHM) in the EL spectra, we can reasonably correlate the integrated EL intensity to absolute EL intensity at the center emission wavelength. It is clear that LEDs with a HT (high-temperature)- or LT (low-temperature)-InAlN EBL (Table 2) show higher EL intensities in both integrated and absolute values compared to the LED without an InAlN EBL. This result indicates that the InAlN EBL is effectively confining electrons by preventing them from escaping the MQWs, leading to the improved quantum efficiencies in the active-region-friendly green LEDs. The LEDs with HT- and LT-InAlN EBLs are ~22 % and ~50 % brighter than the LED without EBL, respectively, at a current density of $J$=65.3 A/cm$^2$. Comparing

luminous efficiencies between the LEDs with HT-EBL and LT-EBL, the integrated EL intensity of LEDs with the LT-InAlN EBL was 30% brighter than that of LEDs with the HT-InAlN EBL for $J$=40.8 A/cm$^2$. This observation can be explained by the difference in optical quality of InGaN/GaN MQW active region depending on thermal budget, *i.e.*, temperature and duration time, during the growth of *p*-type layers. The results and further discussion were reported in detail in ref. 35.

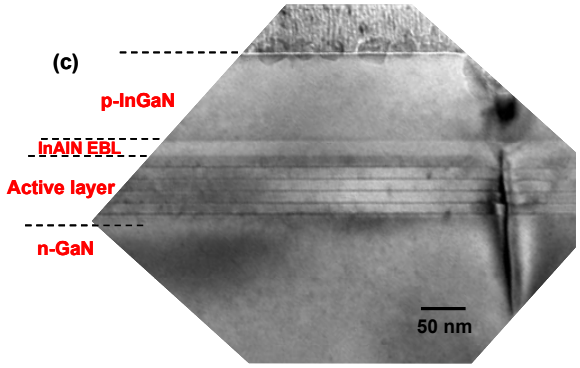


Figure 18: Cross sectional TEM image of green LED structure with InAlN EBL.

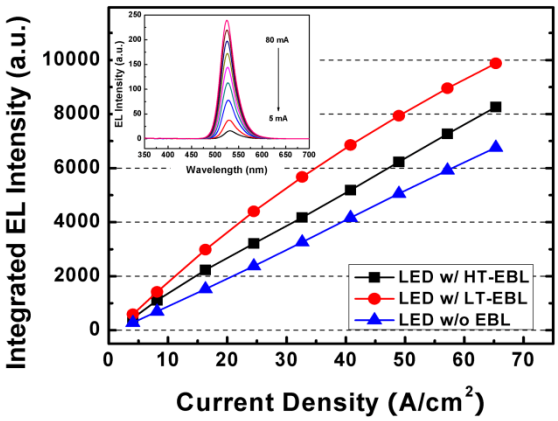


Figure 19: Light output vs. current (*L-I*) curve of green LEDs (a) without EBL, (b) with HT-InAlN EBL, and (c) with LT-InAlN EBL; inset shows electroluminescence spectra of green LEDs with LT-InAlN EBL.

Table 2: Description various InAlN electron blocking layers (EBLs) employed in the green LEDs.

| Sample number | $x_{In}$ in InAlN UL | InAlN EBL (nm) | InAlN $T_g$ (°C) / time (sec) |
|---|---|---|---|
| 1.1596-6 (w/o EBL) | 0 | 0 | N/A |
| 1-1605-6 (w/ HT-EBL) | 0.18 | 20 | 840 / 1500 |
| 1-1604-6 (w/ LT-EBL) | 0.18 | 20 | 780 / 306 |

This efficiency difference between InAlN EBLs can also be explained by carrier (especially holes) transport difference caused by InAlN EBLs. Figure 20 shows cross-section transmission electron micrographs of the device structures with a LT-EBL and a HT-EBL. Both films exhibit well defined InGaN QW layers. However, the crystalline quality of the InAlN EBL is quite different. The LT-EBL is undulated with inhomogeneous strain which may be associated with Stranski-Krastanow growth mode, while the HT-EBL has a uniform thickness and contrast, reflecting a two-dimensional growth. Figure 21 shows the CL spectra for the LEDs with and without an InAlN EBL. We observe that the LT- and HT-EBL devices have comparable QW emission intensities and are about 4 times more intense than the device without EBL. The holes from the *p*-layer can hop through the thinner regions of the EBL into the active region, whereas the holes in the HT-EBL case have to hop through the uniformly thick EBL. From the CL spectra in Figure 21, the introduction of an EBL layer in the film forces the electron-hole pairs, generated in the active region by the electron beam, to recombine radiatively in the QWs, whereas devices without EBL allow some electrons to leak into and recombine in the *p*-layer –

evidenced by the weak emission at ~ 380 nm. It should be noted that in CL, electrons and holes are generated as pairs in the active region, whereas in EL electrons and holes are injected from the *n*- and *p*-regions, respectively. The CL emission intensity observed in the HT-EBL case is higher than in the LT-EBL case. This is consistent with holes being created in the active region, without the need for them to tunnel through the EBL as in the case of injection (EL). This suggests that in the HT-EBL case most of the electrons and holes recombine in the active region due to the reduced carrier leakage through the uniformly thick EBL. The results and further discussion were reported in detail in ref. 36.

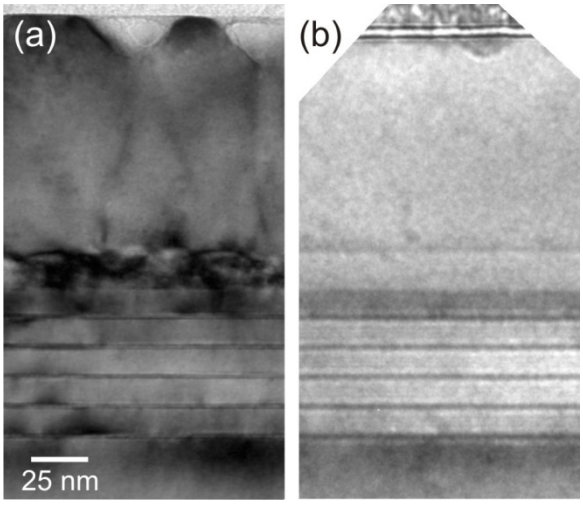


Figure 20: Cross-section TEM of the active region of the (a) LT-EBL and (b) HT-EBL device structures.

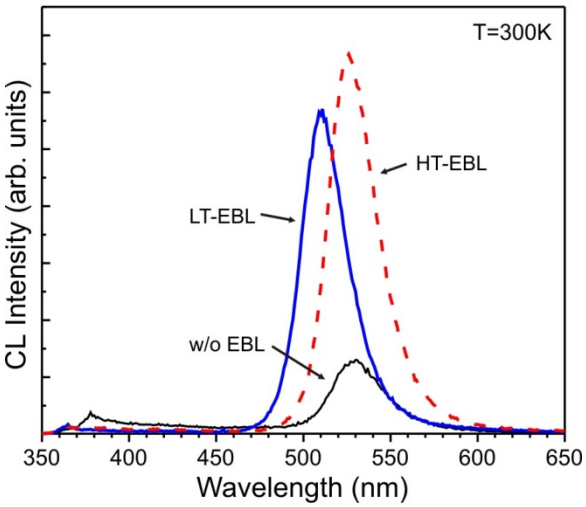


Figure 21: Room-temperature CL spectra of the QW emission of the three films.

In summary, we have proposed and demonstrated, for the first time, a new InAlN EBL. The new EBL is active-layer-friendly in terms of thermal budget and lattice-matched to GaN. We have demonstrated that the InAlN EBL is an effective method for improving the quantum efficiency of green LEDs. This InAlN EBL can also be applied to blue and violet visible LEDs to provide a better electron confinement with lattice matching capabilities.

### *8. Peak efficiency and efficiency droop improvement in blue LEDs with an InAlN electron blocking layer*

*This study includes tasks 1, 2, and 3.1 with a focus on the effect of electron spill-over on the IQE and DE in blue LEDs.*

We compared the luminescence characteristics of blue LEDs with an $In_{0.18}Al_{0.82}N$ EBL, a conventional $Al_{0.2}Ga_{0.8}N$ EBL, and without an EBL, and presented a study of the peak IQE and the ED behavior associated with carrier spill-over, which is suspected to be one of the origins of efficiency droop. In the case of blue LEDs, the epitaxial structures employs conventional *p*-type GaN layer (as opposed to active-region-friendly *p*-type InGaN that we have proposed) grown at higher temperature than that of green LEDs. Therefore, in this study, we investigated the effect of electron blocking behavior (without being affected by thermal budget during the growth of *p*-type layers) on the peak IQE and ED of the LEDs in comparison to conventional AlGaN EBLs.

Figure 22 shows the in-plane lattice constants and bandgap energies of InAlGaN materials suggesting $In_{0.18}Al_{0.82}N$ ternary alloy is lattice matched to GaN while providing wider bandgap than typical AlGaN ($x_{Al}$<0.3) EBLs. Therefore, $In_{0.18}Al_{0.82}N$ EBL can offer higher potential barrier than typical AlGaN EBLs, as shown in Figure 23

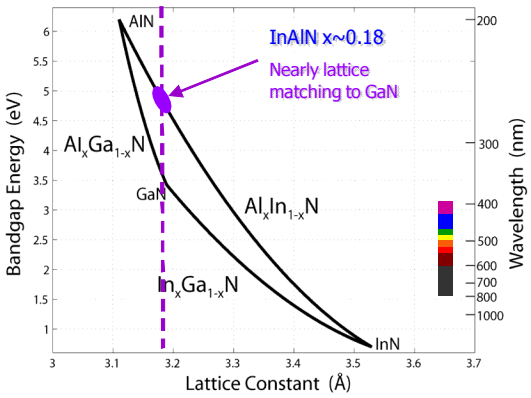


Figure 22: Bandgap energy vs. lattice constant of III-N semiconductor materials showing lattice matching of $In_{0.18}Al_{0.82}N$ to GaN.

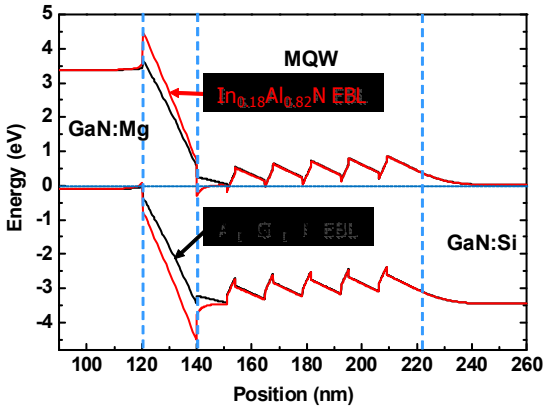


Figure 23: Electronic band diagram of III-N visible LEDs with an $Al_{0.2}Ga_{0.8}N$ EBL and an $In_{0.18}Al_{0.82}N$ EBL.

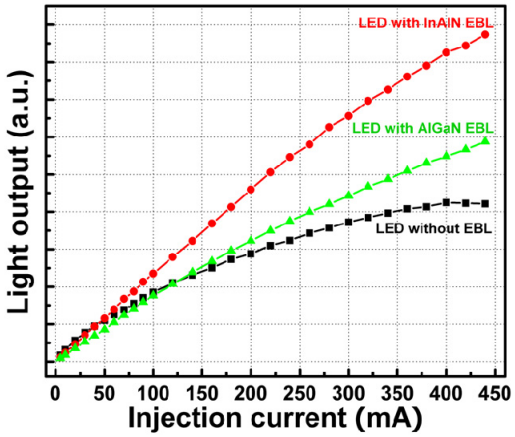


Figure 24: Light output vs. current (*L-I*) characteristics of LEDs without an EBL, with an $Al_{0.2}Ga_{0.8}N$ EBL, and with an $In_{0.18}Al_{0.82}N$ EBL.

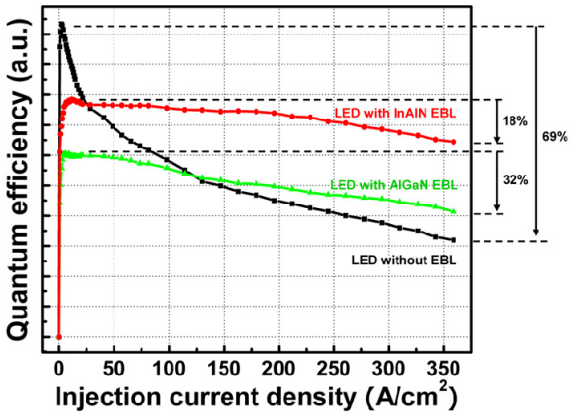


Figure 25: Quantum efficiency vs. current density for the LEDs without an EBL, with an $Al_{0.2}Ga_{0.8}N$ EBL, and with an $In_{0.18}Al_{0.82}N$ EBL.

From EL spectra of the LEDs (not shown here), the peak emission wavelengths at $I$=60 mA of LEDs without an EBL, with an $Al_{0.2}Ga_{0.8}N$ EBL, and with an $In_{0.18}Al_{0.92}N$ EBL were located at ~475 nm, ~476 nm, and ~473 nm, respectively, *i.e.*, did not change very much with the different EBL schemes. The light-emission characteristics of the LEDs were estimated by comparing the integrated intensity change with increasing current, as shown in Figure 24. The LED without an EBL shows, in the low injection current region of $I$<40 mA, an almost linear increase in light output that is slightly higher than the LEDs with EBLs. At higher injection currents, however, *L-I* curve shows a distinct sub-linear behavior and a tendency to saturate at $I$~75 mA. At even higher currents, $I$>360 mA, an increase in the injection current hardly

contributes to the increase of light output, *i.e.*, only a small portion of injected carriers result in radiative recombination. The LED with an $Al_{0.2}Ga_{0.8}N$ EBL shows lower light outputs than the LED without an EBL for low and medium injection currents ($I$<120 mA). However, with an increase of injection current, the light output rapidly increases with injection current and surpasses the LED without an EBL at $I$~140 mA. Moreover, the higher slope of the curve is maintained at higher currents, with a significantly reduced efficiency droop, showing ~25% higher light output at $I$=360 mA and ~40% higher at $I$=440 mA than the LED without an EBL. The light output of the LED with an $In_{0.18}Al_{0.92}N$ EBL is slightly higher than that of the LED without an EBL at $I$=50 mA but it ramps up significantly with increasing injection current. As a result, it is ~110% brighter than the LED without an EBL and 40% brighter than the LED with an $Al_{0.2}Ga_{0.8}N$ EBL at $I$=440 mA. The light output is significantly enhanced when either an $Al_{0.2}Ga_{0.8}N$ or $In_{0.18}Al_{0.92}N$ layer is inserted as an EBL, possibly due to their improved electron blocking effect in the high injection current regime. Also, the higher light output of the LED with an $In_{0.18}Al_{0.92}N$ EBL indicates a superior electron confinement with respect to the $Al_{0.2}Ga_{0.8}N$ EBL case. To clarify the effect of the various EBLs on the efficiency droop, the quantum efficiency of the LEDs is calculated and plotted vs. current density in Figure 25. After a rapid increase at very low injection current densities, all the LEDs show a monotonic efficiency drop with increasing current. The efficiency droop can be defined by the ratio of drop of efficiency from the peak value. The LED without an EBL shows a sharp peak efficiency at $J$=3 A/cm$^2$, while the LEDs with an $Al_{0.2}Ga_{0.8}N$ EBL and an $In_{0.18}Al_{0.92}N$ EBL show peak efficiencies at $J$=6 A/cm$^2$ and 11.5 A/cm$^2$, respectively. Note that the peak efficiency of the LED without an EBL is higher than other LEDs with EBLs and also occurs at lower current density. The insertion of an EBL creates barriers not only in the conduction band, but also in the valence band that may act as a hole-blocking barrier. At low current densities, this barrier may limit the hole transport into the active region and may result in non-uniform hole distribution, leading to lower quantum efficiencies for LEDs with an EBL than for LEDs without an EBL. Beyond the peak efficiency, the LED without an EBL shows a rapid efficiency drop with increasing injection current density, suggesting severe carrier loss by spill-over. The quantum efficiency of the LED without an EBL at $J$=360 A/cm$^2$ is only one-third of its peak efficiency value, showing an efficiency droop of ~69%. On the other hand, the LED with an $Al_{0.2}Ga_{0.8}N$ EBL shows the lowest peak efficiency at low current densities, but the droop of efficiency with an increase of current density is much smaller than that of the LED without an EBL. As a result, its quantum efficiency exceeds that of the LED without an EBL at current density higher than $J$=130 A/cm$^2$, and show a ~30% higher quantum efficiency at $J$=360 A/cm$^2$. The efficiency droop is also improved, with only a ~32% efficiency drop at $J$=360 A/cm$^2$ with respect to the peak value. The peak efficiency of the LED with an $In_{0.18}Al_{0.92}N$ EBL is located between those of the LEDs with an $Al_{0.2}Ga_{0.8}N$ EBL and the LED without an EBL, and due to its smallest efficiency drop rate, it shows the highest absolute efficiency and the lowest efficiency droop at high current densities. The efficiency droop at $J$=360 A/cm$^2$ is estimated to be ~18% compared to its peak value. Thus, the $In_{0.18}Al_{0.92}N$ EBL has demonstrated to provide a better electron blocking effect than the $Al_{0.2}Ga_{0.8}N$ EBL, and the LED with an $In_{0.18}Al_{0.92}N$ EBL shows significantly improved emission intensities and substantially mitigated efficiency droop in visible LEDs than the LEDs with conventional $Al_{0.2}Ga_{0.8}N$ EBLs. However, although the ED is significantly improved by the InAlN EBL by minimizing carrier spill-over, the droop is not completely suppressed. This may suggest that other mechanisms such as Auger recombination,

limited hole transport, etc., also have some influence in the ED. Alternatively, even $In_{0.18}Al_{0.82}N$ EBL cannot provide enough potential barrier to completely suppress the carrier spill-over. The results and further discussion were reported in detail in ref. 37.

In summary, we demonstrated that the use of an InAlN EBL is an effective way to reduce the ED in III-N visible LEDs. A significant enhancement of the EL intensity and light output in blue LEDs with an $In_{0.18}Al_{0.92}N$ EBL over similar LEDs without an EBL and with an $Al_{0.2}Ga_{0.8}N$ EBL was demonstrated. Also, it has been shown that an $In_{0.18}Al_{0.92}N$ EBL is more effective than a conventional $Al_{0.2}Ga_{0.8}N$ EBL in improving IQE and reducing ED at high injection current densities by carrier spill-over.

### *9. Effect of hole transport and resulting carrier distribution in MQWs of III-N LEDs*

*This study includes tasks 1, 2, and 3.1 with a focus on the effect of hole transport on the IQE and DE in visible LEDs.*

In the section 4 of the "results and discussion" in this report, we discussed non-uniform distribution of holes among MQWs. We have also proposed that the limited hole injection can limit the peak IQE and is related to the ED.[15] Following reports suggest that the uniform carrier distribution in the MQW active region can mitigate the ED.[16] In order to accomplish uniform hole distribution, effective hole transport is considered to be a key factor. The limited hole transport into the active region and the non-uniform hole distribution among the MQWs result not only from the relatively large effective hole mass but also from the specific characteristics of the QWs, QWBs, and EBLs, such as potential barrier height, thickness, and doping of those layers. The engineering of MQW design for the improvement of efficiency droop behavior is, however, in many cases, limited by the fact that it is often achieved at the expense of peak IQE of the LEDs. As the ED is defined by the ratio of QE value at high current density to the maximum QE value (or to QE value close to the maximum QE) at low current density, the droop ratio could appear to be improved by sacrificing the latter. Therefore, the improvement in efficiency droop without sacrificing QE at relatively low current levels is important when mitigating the efficiency droop problem.

In this study, we focus on the engineering of carrier dynamics by altering the nature of layers that do not belong to the active region. We report on the effect on hole transport into the active region and resulting hole distribution among the MQWs by controlling In mole fraction of *p*-type $In_xGa_{1-x}N$:Mg layers in the LED structures. In particular, we employed triple-wavelength (TW)-emitting MQW design having different In mole fractions so that each QW emits its own characteristic wavelength that can be used to experimentally evaluate the transport and distribution of holes in the active region. In addition, silicon (Si) doping was introduced in a selected QB to intentionally control the hole transport in MQW active region. The *p*-$In_xGa_{1-x}N$ layers have In mole fractions ($x_{In}$) of 1.5%, 2.5% and 3.5% and they are labeled as LED A, LED B, and LED C, respectively. TW-MQWs consist of violet (λ~420 nm), blue (λ~460 nm), and cyan (λ~500 nm) QWs, designated as QW1, QW2, and QW3, respectively, in a sequence of epitaxial growth so that the QW1 having the widest band gap was located close to the *n*-GaN:Si layer and the QW3 having the narrowest band gap was placed close to the *p*-$In_xGa_{1-x}N$:Mg layer.

XRD $\omega$-$2\theta$ scans (data not shown here) of the TW-LED epitaxial structures with *p*-$In_xGa_{1-x}N$:Mg layers are similar except for the location of the peak corresponding to *p*-$In_xGa_{1-x}N$ layer near the GaN peak, indicating that the structure of MQW active region including the composition and the thickness of QWs and QWBs are essentially the same for the LEDs A, B, and C, which

can rule out the possibility of the composition and thickness effects of the MQW active region on the hole transport behavior. In addition, PL spectra (data not shown here) of three TW-LED structures confirmed the presence of separated QW layers. The similar shapes of PL spectra and each PL peak wavelength in the MQW region support the identical active region structures and optical quality of the LEDs A, B, and C.

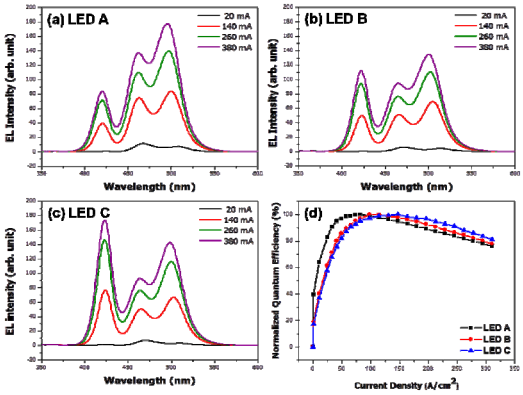


Figure 26: EL spectra of (a) LED A, (b) LED B, and (c) LED C as a function of injection current, and (d) normalized quantum efficiency of the LEDs A, B, and C. LEDs A, B, and C have $p$-$In_xGa_{1-x}N$:Mg layers with $x_{In}$ = 1.5%, 2.5%, and 3.5%.

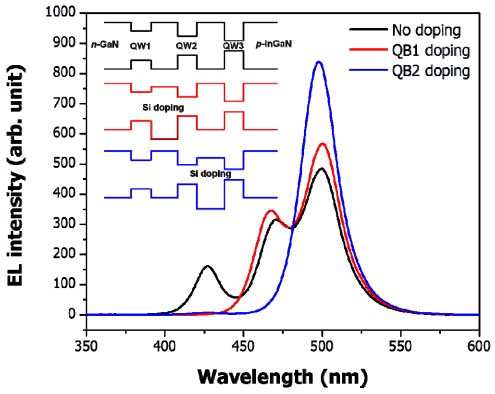


Figure 27: EL spectra of TW-LEDs employing a $p$-$In_{0.025}Ga_{0.975}N$ layer with Si doping in a selected QWB. Inset shows the location of Si doping in a selected QB.

Electro-optical characteristics of the wafer-level (without packaging) TW-LEDs were measured from the substrate side in order to minimize absorption by narrower QW. The photon recycling effect is expected to be negligible. The electroluminescence (EL) spectra for the three LEDs are shown in Figure 26. We compare them to investigate the hole transport behavior depending on the injection current in a pulse-mode to minimize Joule heating. The EL peak wavelengths for QW1, QW2, and QW3 at $I$=20 mA are λ=423, 467, and 508 nm for the LED A, λ=424, 470, and 512 nm for the LED B, and λ=424, 470, and 509 nm for the LED C, respectively, which suggests the peak emission wavelength was not significantly affected by the difference in $p$-$In_xGa_{1-x}N$:Mg layers. For the LED A in Figure 26 (a), QW2 and QW3 having blue and cyan characteristic colors show stronger emission than QW1 with violet color. In addition, although the EL peak intensities of all three QWs increases with injection current, the EL peak of QW1 shows lower intensity than those of QW2 and QW3 for the entire injection current range. Assuming the distribution of electrons among TW-QW is rather uniform, this should be related to the distribution of holes available for radiative recombination, and indicates that the upper QWs adjacent to $p$-$In_xGa_{1-x}N$:Mg layer do emit more photons. Holes have a higher effective mass than electrons (*e.g.*, 1.1 $m_0$, compared to 0.2 $m_0$ for electrons in GaN-based materials) and corresponding low mobility so that it is difficult for hole transport into the lower QWs far away from $p$-$In_xGa_{1-x}N$:Mg layer. However, Figure 26 (b) shows that for the LED B the emission from QW1 becomes stronger at the expense of that from QW2 and QW3. The peak intensity of QW1 becomes comparable to that of QW3 above $I$ ~ 140 mA. This result suggests that in the case of the LED B more holes injected into the active region were transported to QW1 from QW2 and QW3 compared to the LED A. The enhanced hole transport is more clearly

shown in the LED C having the highest In mole fraction in the *p*-$In_xGa_{1-x}N$:Mg layer. As shown in the Figure 26 (c), the EL intensity of QW1 is higher than those of QW2 and QW3 even at relatively low injection currents as well as at high driving currents up to *I*~380 mA. Moreover, the QW1 in LED C shows the highest EL intensity among the three TW-LEDs over the entire injection current range. This gradual increase in EL intensity of QW1 from LED A to LED C and stronger emission of QW1 compared to QW2 and QW3 in LED C indicate that more holes can be transported to the lower QW as drive current increases. Since the MQW epitaxial layer design and growth conditions for the LEDs A, B, and C were identical, it is reasonable to infer that the changes of emission spectra from the LED A to the LED C were induced by improved hole transport by varying the In mole fraction of *p*-$In_xGa_{1-x}N$:Mg layer.

In order to further confirm the hole transport effect, Si doping in a selected QWB is employed, as shown in the inset of Figure 27, since the intentional Si doping in a QWB is an effective way to block the hole transport by enhancing a potential barrier for the balance band of electronic band structure.[33] Figure 27 shows the EL spectra of TW-LEDs having a *p*-$In_{0.025}Ga_{0.975}N$ layer (similar to the LED B but not the same samples) with Si doping in a selected QWB. The Si doping is estimated to be $n$~$5\times10^{18}$ $cm^{-3}$. When the QWB between QW1 and QW2 (QB1/2) is doped with Si, the emission from QW1 disappears due to further limited hole transport into QW1. Moreover, there is only one strong emission from QW3 in the case of the TW-LED with Si doping of QWB2/3 (QWB between QW2 and QW3). This results further supports that the gradually increased EL intensity of QW1 from LED A to LED C is caused by improved hole transport in the MQW active region increasing the In mole fraction of the *p*-$In_xGa_{1-x}N$:Mg layer. This improvement in hole transport may be due to strain effects in the *p*-type region by $In_xGa_{1-x}N$, or to modified kinetic energy of holes by a potential barrier between the *p*-$In_xGa_{1-x}N$ and the GaN in the last QB. The results and further discussion will be reported in detail in ref. 38.

In summary, enhanced hole transport with increasing In mole fraction in the *p*-$In_xGa_{1-x}N$:Mg layer has been shown. The improved QE and ED at the high current density can possibly be achieved by enhanced hole transport resulting from increasing the In-mole fraction in the *p*-$In_xGa_{1-x}N$:Mg layer, resulting in a hole transport favorable environment in the MQW active region.

### *10. Efficiency droop by electron spill-over and hole injection in visible III-N LEDs*

*This study includes tasks 1, 2, and 3.1 with a focus on the effect of electron spill-over and hole transport on the ED in visible LEDs.*

In the section 8 of the "results and discussion" in this report, we discussed improved IQE and mitigated ED in visible LEDs by InAlN EBLs. In addition to the practical benefit of the performance improvements, a lattice-matched EBL can offer insight into the nature of carrier spill-over and limited hole injection efficiency. The $In_{0.18}Al_{0.82}N$ layer can control electron confinement and hole transport without side effects. In the case of $Al_xGa_{1-x}N$ EBLs with different aluminum (Al) mole fractions to change the heights of the electron and hole potential barriers, *p*-type doping efficiency of the EBL as well as the strain in the EBL is changed in addition to the intended barrier height control. Different *p*-type doping in the EBL can significantly affect the hole injection efficiency on top of the effect of the hole transport barrier. Even for the same Al mole-fraction AlGaN EBLs with different thicknesses, the layers possess different strain energies, thus apply different strain status to the heterostructure. Therefore, we

use in-plane lattice-matched InAlN EBLs with different thickness to study the efficiency droop contributions due to both electron spill-over and limited hole-injection efficiency in the absence of strain and doping effects.

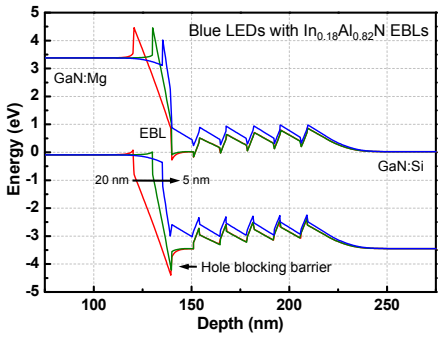


Figure 28: Electronic band diagram of blue LED epitaxial structures with $In_{0.18}Al_{0.82}N$ EBLs with thicknesses of 5, 10, and 20 nm.

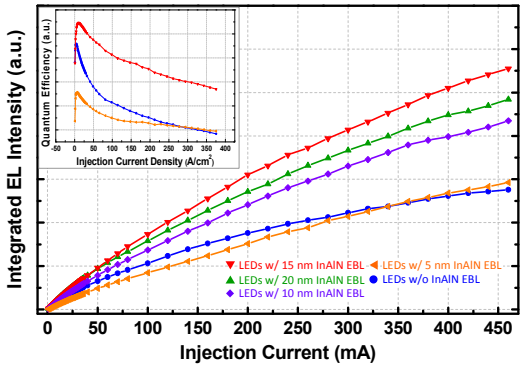


Figure 29: Light output vs. current (*L-I*) and selected (for EBL thickness of 0, 5, and 15 nm) corresponding QE vs. injection current density (inset) of the LEDs with $In_{0.18}Al_{0.82}N$ EBLs with various thicknesses.

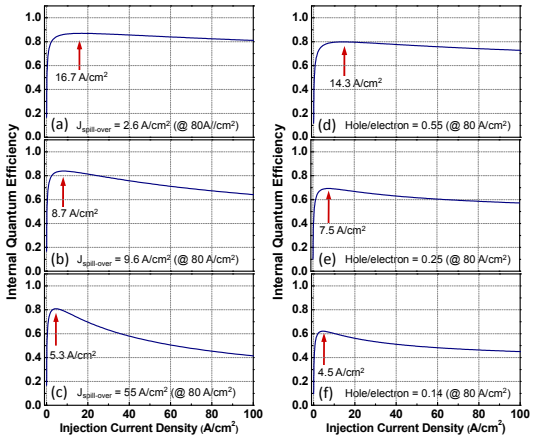


Figure 30: Calculated QE vs. injection current densities of LEDs for various spill-over currents ((a), (b), and (c)) and hole/electron concentration ratios ((d), (e), and (f)).

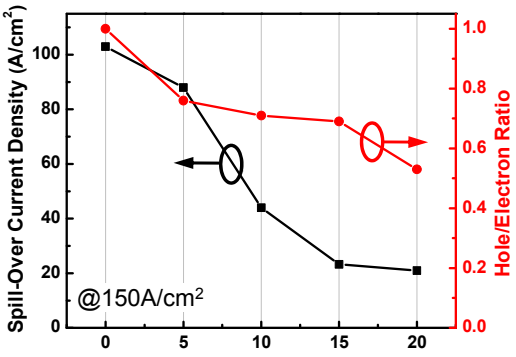


Figure 31: Calculated spill-over current density and hole/electron concentration with various thicknesses of $In_{0.18}Al_{0.82}N$ EBLs at an injection current density of 150 A/cm$^2$.

Figure 28 shows the equilibrium electronic band diagram of blue LED structures with $In_{0.18}Al_{0.82}N$ EBLs having different thicknesses. The potential barrier in the valence band is present between the *p*-GaN and the active region to reduce the hole-injection efficiency. By decreasing the EBL thickness from 20 nm to 5 nm, the calculated barrier height is decreased at the expense of the reduced electron confinement effect in the conduction band by decreasing width and height of the potential barrier. This trade-off suggests that the optimum LED performance should be achieved by balancing the effects of electron confinement in the active

region and hole transport into the active region. In this study, the luminous performance of the blue LEDs with different $In_{0.18}Al_{0.82}N$ EBLs is measured, and their QE curves are theoretically calculated to determine the relative contributions of carrier spill-over and the hole-blocking effects to the ED of III-N visible LEDs.

Figure 29 shows the light output vs. current (*L-I*) and the selected corresponding QE as a function of the injection current density (inset) for the wafer-level (without packaging) LEDs. All the LEDs show a typical *L-I* and QE behavior with a rapid increase in QE at low injection currents and then a steady decrease at high injection currents. Several features are worth noting: First, the LEDs with a 5-nm EBL show lower QE (lower light output) than the LEDs without an EBL except at very high current densities ($J$>300 A/cm$^2$). Also, the LEDs with a 20-nm EBL generally show lower light output than the LEDs with a 15-nm EBL. If only the electron blocking effect is taken into account, these results, especially for the latter case, cannot be explained, because the insertion of the EBL or the increase of its thickness is supposed to reduce (if not suppress) the carrier spill-over. In addition, the current density where the peak QE appears ($J_{peakQE}$) has a trend with the EBL thickness, *i.e.*, $J_{peakQE}$=5, 6, and 13 A/cm$^2$ for the LEDs with 5-, 10-, 15-nm EBLs. The peak efficiency at low current densities has been reported to be related to defect-related non-radiative Shockley-Read-Hall (SRH) recombination. However, since all the LED structures in this study share the same growth condition and crystalline quality in the GaN buffer and MQW active region, the SRH and radiative recombination coefficients are expected to be same at least at similar current densities, even considering a carrier delocalization effect. In addition, it was observed that the value of the injection current at the peak efficiency is closely related with the carrier spill-over and the hole-injection efficiency. Therefore, different carrier dynamics influenced by the different InAlN EBL structures is considered to be a more probable cause for the variation in peak QEs and their injection currents. For a theoretical study of the QE curves, we extended the *ABC* model to include carrier spill-over and hole-injection effects. The spill-over effect was taken into account as carrier losses. As a result, the injection current density can be written as

$$\frac{J - J_{spill-over}}{qd} = An + Bn^2 + Cn^3 + \frac{J_{spill-over}}{qt} \quad (1)$$

where $n$ is the carrier density, and $A$, $B$, and $C$ represent the rate coefficients of SRH, radiative, and Auger recombinations, respectively. $J_{spill-over}$ is the spill-over current density caused by the carrier spill-over, $d$ is the thickness of the active region, and $t$ is the diffusion length of spilled carriers. The spill-over current density can be expressed as **Error! Bookmark not defined.**

$$J_{spill-over} = kJ^b \quad (2)$$

where $k$ and $b$ are constants. We used $1.0\times10^7$ s$^{-1}$, $2.0\times10^{-10}$ cm$^3$s$^{-1}$, and $4.0\times10^{-30}$ cm$^6$s$^{-1}$ for $A$, $B$, and $C$, respectively. The IQE is then represented as

$$\eta = \frac{Bn^2}{An + Bn^2 + Cn^3 + J_{spill-over}/qt} \quad (3)$$

In addition, the effect of the hole blocking resulting in the decrease of hole injection efficiency was included in the model as a reduction of the hole concentration with respect to the electron concentration in the active region. The ratio between the excess hole concentration ($\Delta p$) and the excess electron concentration ($\Delta n$) was calculated using the Fermi-Dirac function to have the hole concentration, $p$ (~$\Delta p$, as $\Delta p >> p_0$, $p_0$ is an equilibrium hole concentration) being smaller

than the electron concentration, $n$ (~$\Delta n$) at low injection conditions, but becoming similar to $n$ at high injection conditions, as follows:

$$\frac{\Delta p}{\Delta n} = \frac{1}{1+\exp((F-\Delta n)/G)} \quad (4)$$

where $F$ and $G$ are constants. The hole concentration was included in the rate equations of recombination processes to reflect the local charge imbalance to calculate bimolecular radiative recombination rate, $R=B\Delta n\Delta p$ instead of $R=Bn^2$ ($\approx B(\Delta n)^2$) and Auger recombination rate, $U_{Auger}=C(\Delta n)^2\Delta p$ instead of $U_{Auger}=Cn^3$ (assuming electron excitation to a higher level in the conduction band).

The influence of the spill-over current density and the reduced hole concentration on the shape and peak position of the QEs are representatively estimated by using this model (Eq. (3) in combination with Eq. (2) and (4)). Figure 30 (a), (b), and (c) show the change in the calculated QE curves for various spill-over current densities, with other parameters fixed, including the recombination rate coefficients (same as aforementioned values) and no reduced hole concentration ($G>>F$ in Eq. (4)). Figure 30 (a) shows a QE curve with small carrier spill-over effect ($k$=0.0015 and $b$=1.7 in Eq. (2) to have $J_{spill\text{-}over}$=2.6 A/cm$^2$ at $J$=80 A/cm$^2$). Figure 30 (b) and (c) represent increased spill-over effect with $k$=0.0015 and $b$=2.0, and $k$=0.0015 and $b$=2.4 to simulate moderate and significant spill-over effects, *e.g.*, $J_{spill\text{-}over}$=9.6 and 55 A/cm$^2$ at $J$=80 A/cm$^2$, respectively. The QE curve reaches its peak efficiency at higher injection current densities under lower spill-over current conditions (Figure 30 (a)) and peak efficiency position moves toward lower current densities with increasing spill-over currents (Figure 30 (b) and (c)). Also, the QE curves for the LEDs with high spill-over current show more pronounced droop behaviors in the efficiency with the increase of the injection current. Figure 30 (d), (e), and (f) show the effect of hole injection with a fixed spill-over condition ($k$=0.0015 and $b$=1.7 to simulate, *e.g.*, $J_{spill\text{-}over}$=2.6 A/cm$^2$ at $J$=80 A/cm$^2$) for increased hole-blocking effects with varied $F$ and $G$ to simulate the ratios of hole concentration to electron concentration to be 0.55, 0.25, and 0.14 at a current density of $J$=80 A/cm$^2$. The calculation shows the similar trend with moving of the peak efficiency position toward lower current densities with lower hole concentrations (or higher hole-blocking conditions). Also, efficiency droop is predicted but less significant than the effect of electron spill-over, when comparing two sets of conditions in this study. Instead, the difference in values of the peak efficiency depending on hole concentration appears to be more pronounced than that depending on spill-over conditions. Thus, the shape and the QE peak position are affected by the relative hole concentration as well as by the spill-over current density. This result indicates that an LED structure with a low hole concentration has a QE peak position at a lower current density even when the spill-over current is very small. The observation that the QE peak position of the LED with a 20-nm EBL ($J_{peakQE}$=10 A/cm$^2$) is located at a lower current density than the LEDs with a 15-nm EBL ($J_{peakQE}$=13 A/cm$^2$) can be accounted by considering the change of the hole concentration caused by the EBL overshadowing carrier spill-over current change.

For more detailed analysis on the electron-confinement and the hole-blocking effects of the InAlN EBLs, the QE curves of the LEDs were numerically fitted using our extended *ABC* model. The spill-over current density and the excess hole concentration with respect to excess electron concentration are calculated from the fitting parameters. In Figure 31, the calculated spill-over current density and the hole/electron concentration ratio vs. EBL thickness are plotted at a typical current density of $J$=150 A/cm$^2$. The spill-over current density and hole/electron ratio in

Figure 31 show a similar trend: they decrease with increasing EBL thickness but at different rates. For example, the LEDs with a 20-nm EBL have a slightly reduced spill-over current density but a much lower hole concentration (or much higher hole-blocking effect) than the LEDs with a 15-nm EBL. The observation in the inset of Figure 29 that the LEDs with a 5-nm EBL have lower QE than the LEDs without an EBL can be explained by the calculations in Figure 31, showing that the LEDs with a 5-nm EBL have a slightly lower spill-over current density but a significantly lower relative hole concentration than the LEDs without an EBL. This estimation is consistent with the experimental observation that light output of the LEDs with a 5-nm EBL surpasses that of the LEDs without an EBL only when the current density reaches at very high injection regions. Therefore, the spill-over current density and the relative hole concentration obtained by the model is in good agreement with the QE measurements. The highest efficiency and light output observed in Figure 29 for the LEDs with a 15-nm $In_{0.18}Al_{0.82}N$ EBL, can be explained by a low spill-over current but a relatively less reduced hole concentration in the active region. The results and further discussion will be reported in detail in ref. 39.

In summary, the EL measurements of the LEDs showed that LEDs with a 15-nm $In_{0.18}Al_{0.82}N$ EBL have the highest QE. The model suggests that the high electron-confinement and the relatively low hole-blocking effects by the 15-nm $In_{0.18}Al_{0.82}N$ EBL is the main reason for the high QE and reduced ED effects. The study also suggests that the hole-blocking and the electron-confinement effects of the EBL should be qualitatively considered to obtain higher light output and efficiency performance for LEDs operating at high current densities.

### *11. Effect of InGaN underlayer*

*This study includes tasks 1 and 2 with a focus on fundamental nature of structural and optical properties of MQW affected the InGaN underlayer that can be used in visible LEDs.*

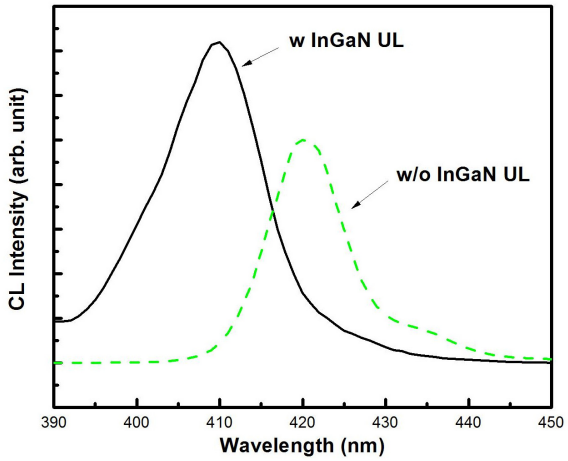


Figure 32: CL spectra of the MQW emission measured at a temperature of 4.5 K with an electron accelerating voltage of 4 kV for layer structures with and without the $In_{0.03}Ga_{0.97}N$ underlayer.

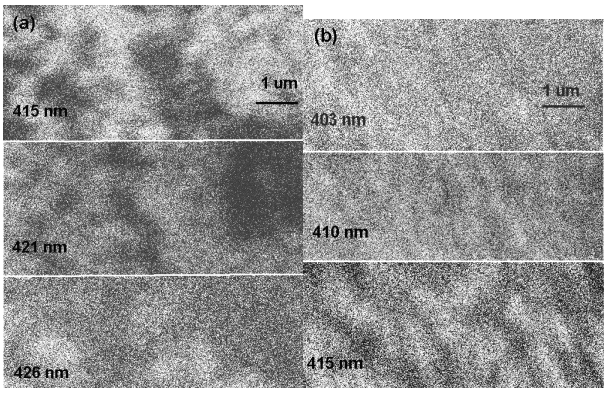


Figure 33: Monochromatic CL images taken at different wavelengths for layer structures (a) without and (b) with $In_{0.03}Ga_{0.97}N$ underlayer.

Figure 32 shows the CL spectra taken at liquid helium temperatures for the InGaN QWs structure with and without an $In_{0.03}Ga_{0.97}N$ underlayer. For the sample with the InGaN

underlayer, a main peak emission at λ~410 nm (3.024 eV) with a FWHM of 72 meV is observed. There is a 10 nm blue shift with respect to the case without the InGaN underlayer. The internal field due to strain-induced piezoelectric and spontaneous polarization fields results in a spatial separation of electrons and holes in the QW, and causes a red shift in the emission energy. Thus, the blue shift in the QW emission can be explained by a reduction of strain in the QWs by the InGaN underlayer. Monochromatic CL images taken at various wavelengths for both cases are shown in Figure 33. The sample without an InGaN underlayer exhibits a large spatial variation of the QW luminescence, and a complementary contrast is observed between the images taken at the higher and lower energy shoulder of the QW emission peak. This complementary contrast indicates inhomogenous distribution of indium composition in the QW plane. The bright and dark contrasts at λ~415 nm in Figure 33 (a) can be attributed to indium-poor and indium-rich regions, respectively. On the other hand, for the sample with the InGaN underlayer in Figure 33 (b), the spatial inhomogeneity is greatly reduced, and a more uniform luminescence is observed. This can be explained by more uniform indium incorporation due to a lesser strain in the QW layers. In order to further explore the influence of the InGaN underlayer on the optical properties of the active region, time-resolved CL was performed on both samples. Figure 34 shows luminescence transients taken at the QW emission peak, using a pulsed electron beam of 100 ns width at a 100 kHz repetition rate. After the electron beam is switched on at t = 0 ns, the luminescence intensity builds up, eventually reaching a quasi-steady state. At t= 100 ns, the electron beam is switched off and decay in luminescence is observed. The recombination lifetime can be extracted from the transient by fitting the luminescence decay with a single exponential function. The sample with the InGaN underlayer exhibits a much shorter recombination lifetime (10 ns) than the sample without the InGaN underlayer (29 ns). This decrease in lifetime can be explained by the reduction of the internal field in the QWs which enhances the overlap of electron and hole wave functions, thus increasing the radiative recombination rate.

In order to understand the effect of the InGaN underlayer on the QW emission, we used a transmission electron microscope equipped with a biprism for EH measurements to profile the electrostatic potential across the QWs. The electrostatic potential energy across the QWs is shown in Figure 35 for layer structures with and without the InGaN underlayer. Due to a limited field of view in EH, only the bottom three QWs are shown. The electrostatic potential energy was calibrated by using the QW emission energies from the CL measurements combined with a self-consistent 1-D Schrödinger simulation and XRD measurements (not shown here). As shown in Figure 35(a), the QWs exhibit a non-uniform potential profile along the growth direction. The conduction band offset and the internal field in the QWs on the right in Figure 35(a) average 0.32 eV and 0.66 MV/cm, respectively. The left QW (bottom QW in the growth direction) shows different characteristics than the other two QWs. The difference can be explained by a lower indium incorporation in the left QW or, and most likely, due to free-electron tunneling from the InGaN underlayer. These electrons can partially fill the QW and screen the internal field, thus we observe a reduced conduction band offset and a weaker internal field in the left QW. The accumulation of electrons in the left QW may lead to an enhancement of hole injection into the other QWs which may contribute to their observed higher luminescence intensity and efficiency. For the sample without the InGaN underlayer, the electric field inside the QWs is ~ 0.83 MV/cm and quite uniform among the three QWs shown in Figure 35(b). This is consistent with the CL

observation that the emission from the sample without the InGaN underlayer has lower emission energy. The results and further discussion will be reported in detail in ref. 40.

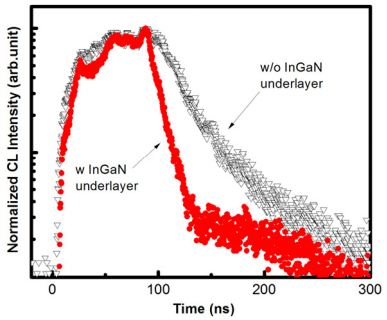


Figure 34: Time-resolved CL transients for the peak energy of the MQW emission. Solid circles represent the transient for the MQWs with the $In_{0.03}Ga_{0.97}N$ underlayer, and open triangles represent the transient for the MQWs without the $In_{0.03}Ga_{0.97}N$ underlayer.

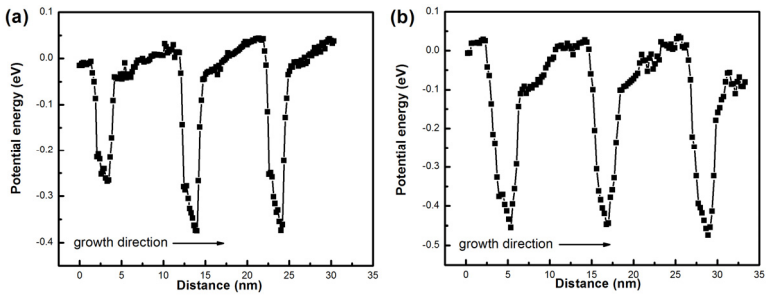


Figure 35: Electrostatic potential across the top QWs determined by electron holography for layer structures (a) with and (b) without $In_{0.03}Ga_{0.97}N$ underlayer.

In summary, a blue shift of emission energy and a reduced recombination lifetime due to the reduction of internal fields have been observed when using InGaN underlayers, which is in part responsible for the improved emission efficiency. EH potential profiles also show an overall reduction of internal fields which is consistent with the optical results. Additionally, in the layer structure with the InGaN underlayer the first QW exhibits a different potential profile than the other QWs, which we interpret to be associated with tunneling of electrons from the underlayer. These characteristics contribute to the reduction of the internal field and the increased luminescence intensity.

### *12. Plan changed and remaining studies*

The research activities in this program were supposed to involve collaborations with industrial partners such as Luminus Devices and Kyma Technologies and their contribution to the program were to be the development of high-power large-area LED chips (Task 3.2) and FS-GaN substrates with various orientations including non-polar and semi-polar directions (Task 4), respectively. However, the plan had been changed and Luminus and Kyma were not involved in the program. As a result of the change, the tasks 3.2 and 4 were not effectively performed. Therefore, among following tasks and milestones, some of them have to be changed and restated:

<u>Tasks</u>

Task 1.0: Growth of High-Quality III-N Emitter Structures (Dupuis, Ryou)
Task 2.0: Detailed Characterization of III-N Light-Emitting Diode Structures
Subtask 2.1: Advanced Material Characterization of III-N MQW LEDs (Ponce)
Subtask 2.2: Conventional Material Characterization for III-N MQW LEDs (Dupuis, Ryou)
Task 3: Design, Processing and Testing of III-N LEDs
Subtask 3.1: LED Device Processing and Testing (Ryou)

Subtask 3.2: LED Device Processing and Testing for High-Power PhlatLight LEDs (Luminus): Not performed

Task 4: Free Standing Bulk GaN Substrate Development (Kyma): Not performed

Program Milestone

Demonstrate fully processed III-N strain and polarization-engineered LEDs on bulk GaN substrates; IQE goal of >45% at 525nm and >25% at 540nm: Changed due to the absence of Kyma contribution

Demonstrate high power PhlatLight devices from strain and polarization-engineered LEDs; EQE goal of >35% at 525nm and >20% at 540nm: Changed due to the absence of Luminus effort

Demonstrate non-polar and semi-polar substrates with size 15×15 mm2, defect densities ~1×106 cm-2, orientation control <0.25°, and surface roughness <0.25nm: Not pursued due to the absence of Kyma effort

Instead, Georgia Tech and ASU team focused on the fundamental aspects of visible III-N LEDs with an emphasis of the effect of strain, defects, and polarization in the epitaxial structures and materials on the IQE and ED behavior. Also, the effect of Stokes loss was not actively studied. Accordingly, the program tasks and milestones can be restated as follows with a reference on the IQE and ED roadmap proposed by DoE:

New Tasks

Task 1.0: Growth of High-Quality III-N Emitter Structures (Dupuis, Ryou)

Task 2.0: Detailed Characterization of III-N Light-Emitting Diode Structures

Subtask 2.1: Advanced Material Characterization of III-N MQW LEDs (Ponce)

Subtask 2.2: Conventional Material Characterization for III-N MQW LEDs (Dupuis, Ryou)

Task 3: Design, Processing and Testing of III-N LEDs

Subtask 3.1: LED Device Design, Processing, and Testing (Ryou)

New Program Milestone

Demonstrate fully processed III-N strain and polarization-engineered *efficiency-droop-mitigated* high-brightness and high-power LEDs on sapphire substrates with efficiency droop <15% at 200 A/cm$^2$ in blue spectral region at ~450nm.

As we will describe in the next section, we have demonstrated the ED ratio achieving a new program milestone employing strain- and polarization-engineered LEDs by new EBL structure. While we believe this value is reliable, there could be a further improvement in the peak IQE that can further improve IQE and ED, and consequently output optical power under high power condition. In addition, we have been working on fundamental nature of the ED, investigating a real origin of the ED. As discussed, several possible origins of the ED have been proposed. Each origin has its champions and the data presented in each set of theoretical studies or experiments seem to be logical to support its mechanism; however, they are not consistent with each other and even contradictory in some cases, when comparing many sets of studies. The dominant mechanisms responsible for efficiency droop with a complete unified view have not been identified. The proposed mechanisms are possibly inter-related and coupled each other and they all may partially contribute to the ED. As an example described in the section 10 of "Results and Discussion", we demonstrated that IQE and ED are affected by both electron spill-over and hole injection. The effect of Auger recombination will also be coupled to those carrier

dynamics, since the Auger recombination rate is proportional to carrier densities. We plan to further study in a fundamental way how the suspected primary origins of efficiency droop are interconnected and to identify the "real" major mechanisms of ED, possibly with quantified contributing factors depending on LED structures.

### *13. Highlights of key results*

In order to understand the fundamental technical issues of visible LEDs in peak IQE and ED and to develop the SP (strain and polarization)-engineered LEDs, we have investigated several important technical aspects of LED epitaxial structures and device fabrications in combination with advanced materials and device characterizations. Among the results we have achieved, Figure 25 shows QE of high-efficiency efficiency-droop-mitigated blue LEDs developed in this program with a droop ratio of only ~4.5% at $J$~200A/cm$^2$ ~18% at $J$~360A/cm$^2$.

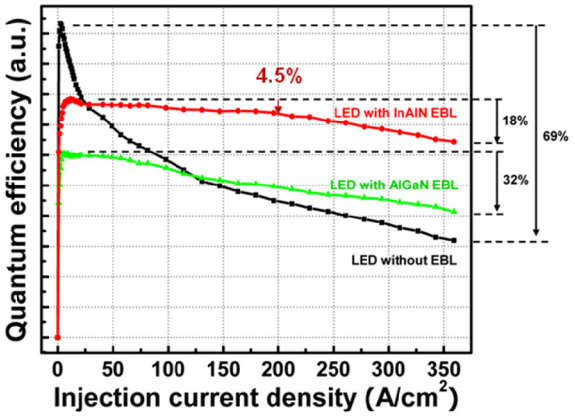


Figure 25: Quantum efficiency vs. current density for the LEDs without an EBL, with an $Al_{0.2}Ga_{0.8}N$ EBL, and with an $In_{0.18}Al_{0.82}N$ EBL.

The technical progresses in this program have been reported in peer-reviewed journals international conference presentations, as shown in bibliography and following is a list of selected publications:

- S. Choi, H. J. Kim, S.-S. Kim, J. P. Liu, J. Kim, J.-H. Ryou, R. D. Dupuis, A. M. Fischer, and F. A. Ponce, "Improvement of peak quantum efficiency and efficiency droop in III-nitride visible light-emitting diodes with an InAlN electron blocking layer," *Appl. Phys. Lett.* **96** (22), 221105-1–3 (2010).
- H. J. Kim, S. Choi, S.-S. Kim, J.-H. Ryou, P. D. Yoder, R. D. Dupuis, A. M. Fischer, and F. A. Ponce, "Improvement of quantum efficiency by employing active-layer-friendly lattice-matched InAlN electron blocking layer in green light-emitting diodes," *Appl. Phys. Lett.* **96** (10), 101102-1–3 (2010).
- J.-H. Ryou, P. D. Yoder, J. P. Liu, Z. Lochner, H. Kim, S. Choi, and H. J. Kim, and R. D. Dupuis, "Control of quantum confined Stark effect in InGaN-based quantum wells," *IEEE J. Select. Topic. Quantum Electron.* **15**, 1080-1091 (2009).
- J. P. Liu, J. Limb, Z. Lochner, D. Yoo, J.-H. Ryou, and R. D. Dupuis, "Green light-emitting diodes with p-InGaN:Mg grown on c-plane sapphire and GaN substrates," *Phys. Stat. Sol. (a)* **206**, 750-753 (2009).

- J. P. Liu, J.-H. Ryou, R. D. Dupuis, J. Han, G. D. Shen, and H. B. Wang, "Barrier effect on hole transport and carrier distribution in InGaN/GaN multiple quantum well light-emitting diodes," *Appl. Phys. Lett.* **93**, 021102-1-3 (2008).

## *CONCLUSION*

We have studied the effects of (1) underlying InGaN layer, (2) tapered and step AlGaN EBL, (3) *p*-$In_xGa_{1-x}N$, (4) *c*-plane FS-GaN substrates, (5) *a*-plane FS-GaN substrates, and (6) new InAlN, which is wide-bandgap and lattice matched to GaN, to understand in a fundamental way the impact of strain, defects, and polarization in relation to unique device structures upon the IQE and ED of III-N light-emitting diodes and to employ this understanding in the design and growth of high-efficiency LEDs capable of highly-reliable, high-current, high-power operation.

We developed high-efficiency and droop-mitigated green and blue LEDs with a new InAlN EBL and plan to further study on the "real" major mechanisms of ED, possibly with quantified contributing factors depending on LED structures.

## *LIST OF ACRONYMS AND ABBREBIATIONS*

| | |
|---|---|
| III-N | III-nitride |
| AFM | Atomic force microscopy |
| arc-s | arc-second |
| CCS | Close-coupled showerhead |
| CL | Cathodoluminescence |
| $Cp_2Mg$ | Bis(cyclopentadienyl)-magnesium |
| *C-V* | Capacitance-Voltage |
| E-beam | Electron beam |
| EBL | Electron blocking layer |
| ED | Efficiency droop |
| EH | Electron Holography |
| EL | Electroluminescence |
| EQE | External quantum efficiency |
| FS-GaN | Free-standing GaN |
| ICP-RIE | Inductively-coupled plasma reactive-ion etching |
| IQE | Internal quantum efficiency |
| *I-V* | Current-Voltage |
| FWHM | Full-width at half maximum |
| LED | Light-emitting diode |
| LD | Laser diode |
| *L-I* | Light-Current |
| MOCVD | Metalorganic chemical vapor deposition |
| MQW | Multiple-quantum well |
| PL | Photoluminescence |
| QCSE | Quantum-confined Stark effect |
| QE | quantum efficiency |
| QW | Quantum well |
| QWB | Quantum well barrier |
| RBS | Rutherford back scattering |
| RTA | Rapid thermal annealing |
| SEM | Scanning electron microscopy (or microscope) |
| SIMS | Secondary ion mass spectroscopy |
| TEGa | Triethylgallium |
| TEM | Transmission electron microscopy (or microscope) |
| TLM | Transmission line measurement |
| TMAl | Trimethylaluminum |
| TMGa | Trimethylgallium |
| TMIn | Trimethylindium |
| TRCL | Time-resolved cathodoluminescence |
| XRD | X-ray diffraction (or diffractometer) |

## *BIBLIOGRAPHY*

Book Chapter

1. Jae-Hyun Ryou, "Chapter 3. GaN and LEDs on sapphire substrates," *Nitride semiconductor LEDs: materials, performance and applications*, J. J Huang, H.-C. Kuo, and S.-C. Shen Ed., Woodhead Publishing, Cambridge, U.K. (manuscript in preparation).

Journal Publication

1. T. Li, Q. Y. Wei, A. M. Fischer, Y. Huang, F. A. Ponce, J. P. Liu, Z. Lochner, J.-H. Ryou, and R. D. Dupuis, "The effect of InGaN underlayers on the electronic and optical properties of visible InGaN/GaN quantum wells," *Appl. Phys. Lett.* (to be submitted for publication).
2. J. Kim, M.-H. Ji, Z. Lochner, S. Choi, J. P. Liu, Md. M. Satter, P. D. Yoder, J.-H. Ryou, R. D. Dupuis, R. Juday, A. M. Fischer, and F. A. Ponce, "Role of p-$In_xGa_{1-x}N$ layer in enhancing hole transport and distribution in InGaN/GaN multiple quantum wells of visible III-nitride light-emitting diodes," *Appl. Phys. Exp.* (submitted for publication).
3. S. Choi, M.-H. Ji, J. Kim, H. J. Kim, Md. M. Satter, J.-H. Ryou, P. D. Yoder, R. D. Dupuis, A. M. Fischer, and F. A. Ponce, "Efficiency droop due to electron spill-over and limited hole transport in III-nitride visible light-emitting diodes employing lattice-matched InAlN electron blocking layers," *Appl. Phys. Lett.* (submitted for publication).
4. J.-H. Ryou and R. D. Dupuis, "Focus Issue Introduction: Optics in LEDs for lighting," *Opt. Exp.* 19 (S4), A897–A899 (2011).
5. S. Choi, H. J. Kim, S.-S. Kim, J. P. Liu, J. Kim, J.-H. Ryou, R. D. Dupuis, A. M. Fischer, and F. A. Ponce, "Improvement of peak quantum efficiency and efficiency droop in III-nitride visible light-emitting diodes with an InAlN electron blocking layer," *Appl. Phys. Lett.* 96 (22), 221105-1–3 (2010).
6. H. J. Kim, S. Choi, S.-S. Kim, J.-H. Ryou, P. D. Yoder, R. D. Dupuis, A. M. Fischer, and F. A. Ponce, "Improvement of quantum efficiency by employing active-layer-friendly lattice-matched InAlN electron blocking layer in green light-emitting diodes," *Appl. Phys. Lett.* 96 (10), 101102-1–3 (2010).
7. A. M. Fischer, K. W. Sun, R. Juday, F. A. Ponce, J.-H. Ryou, H. J. Kim, S. Choi, S.-S. Kim, and R. D. Dupuis, "Effect of growth temperature on the electron-blocking performance of InAlN layers in green emitting diodes," *Appl. Phys. Exp.* 3 (3), 031003-1–3 (2010).
8. S. Choi, H. J. Kim, J.-H. Ryou, and R. D. Dupuis, "Actual temperatures of growing surfaces of III-nitride-based materials depending on substrates and forced convection conditions in metalorganic chemical vapor deposition," *J. Appl. Phys.* 106 (7), 073512-1–6 (2009).
9. J.-H. Ryou, P. D. Yoder, J. P. Liu, Z. Lochner, H. Kim, S. Choi, H. J. Kim, and R. D. Dupuis, "Control of quantum confined Stark effect in InGaN-based quantum wells," *IEEE J. Select. Topic. Quantum Electron.* 15 (4), 1080–1091 (2009).
10. J. W. Lee, C. Sone, Y. Park, S.-N. Lee, J.-H. Ryou, R. D. Dupuis, and H. Kim, "High efficiency GaN-based light-emitting diodes fabricated on inverted-hexagonal-pyramid-mask-embedded structures," *Appl. Phys. Lett.* 95 (1), 011108-1–3 (2009).

11. H. Kim, J.-H. Ryou, R. D. Dupuis, T. Jang, Y. Park, S.-N. Lee, and T.-Y. Seong, "Electrical characteristics of metal contacts to laser-irradiated N-polar n-type GaN," *IEEE Electron Device Lett.* 30 (4), 319–321 (2009).
12. J. P. Liu, J. Limb, Z. Lochner, D. Yoo, J.-H. Ryou, and R. D. Dupuis, "Green light-emitting diodes with p-InGaN:Mg grown on c-plane sapphire and GaN substrates," *Phys. Stat. Sol. (a)* 206 (4), 750–753 (2009).
13. H. Kim, J.-H. Ryou, R. D. Dupuis, S.-N. Lee, Y. Park, J.-W. Jeon, and T.-Y. Seong, "Electrical characteristics of contacts to thin film N-polar n-type GaN," *Appl. Phys. Lett.* 93 (19), 192106-1–3 (2008).
14. J.-H. Ryou, J. Limb, W. Lee, J. P. Liu, Z. Lochner, D. Yoo, and R. D. Dupuis, "Effect of silicon doping in the quantum well barriers on the electrical and optical properties of visible green light emitting diodes," *IEEE Photon. Technol. Lett.* 20 (21), 1769–1771 (2008).
15. J. P. Liu, J.-H. Ryou, Z. Lochner, J. Limb, D. Yoo, R. D. Dupuis, Z. H. Wu, A. M. Fischer, and F. A. Ponce, "Surface morphology control of green LEDs with p-InGaN layers grown by metalorganic chemical vapor deposition," *J. Cryst. Growth* 310 (23), 5166–5169 (2008).
16. J. P. Liu, J.-H. Ryou, R. D. Dupuis, J. Han, G. D. Shen, and H. B. Wang, "Barrier effect on hole transport and carrier distribution in InGaN/GaN multiple quantum well light-emitting diodes," *Appl. Phys. Lett.* 93 (2), 021102-1–3 (2008).
17. J. H. Ryou, W. Lee, D. Yoo, J. B. Limb, R. D. Dupuis, Z. H. Wu, A. M. Fischer, and F. A. Ponce, "Control of quantum-confined Stark effect in InGaN/GaN multiple quantum well active region by p-type layer for III-nitride-based visible light-emitting diodes," *Appl. Phys. Lett.* 92 (10), 101113-1–3 (2008).
18. J. B. Limb, D. Yoo, Y. Zhang, J. H. Ryou, S. C. Shen, and R. D. Dupuis, "GaN ultraviolet avalanche photodiodes grown on 6H-SiC substrates with SiN passivation," *Electron. Lett.* 44 (4), 313–315 (2008).
19. J. P. Liu, J. Limb, J.-H. Ryou, D. Yoo, C. A. Horne, R. D. Dupuis, Z. H. Wu, A. Fischer, F. A. Ponce, A. D. Hanser, L. Liu, E. A. Preble, and K. R. Evans "Blue light emitting diodes grown on free standing (1 1-20) a-plane GaN substrates," *Appl. Phys. Lett.* 92 (1), 011123-1–3 (2008).

Conference Presentation

1. S. Choi, M.-H. Ji, J. Kim, R. Gong, H. J. Kim, Md. M. Satter, P. D. Yoder, J.-H. Ryou, R. D. Dupuis, A. M. Fischer, and F. A. Ponce, "Efficiency droop of III-nitride-based visible light-emitting diodes employing new InAlN electron blocking layers" (MoA2-5), *16th International Conference of Metalorganic Vapor Phase Epitaxy (ICMOVPE XVI)*, Busan, Korea, May 2012.
2. J. Kim, M.-H. Ji, R. Gong, S. Choi, N. Sebhki, Md. M. Satter, P. D. Yoder, J.-H. Ryou, R. D. Dupuis, A. M. Fischer, and F. A. Ponce, "Effect of hole injection layer and electron blocking layer on carrier distribution in III-nitride visible light-emitting diodes" (TuP-18), *16th International Conference of Metalorganic Vapor Phase Epitaxy (ICMOVPE XVI)*, Busan, Korea, May 2012.
3. R. D. Dupuis, J. Kim, S. Choi, M.-H. Ji, J.-H. Ryou, K. W. Sun, A. M. Fischer, and F. A. Ponce, "Effect of electron blocking layer and p-type layer on efficiency droop and hole

transport in InGaN/GaN multiple-quantum-well visible light-emitting diodes" (O4.10), *2011 Materials Research Society (MRS) Fall Meeting*, Boston, Massachusetts, Nov.-Dec. 2011.

4. D. Yuan, R. Guo, J. Kim, M.-H. Ji, S. Choi, J.-H. Ryou, R. D. Dupuis, S. Das, "Enhanced extraction efficiency of GaN-based light-emitting diodes prepared by a combination of metalorganic chemical vapor deposition and laser interference ablation" (K2.4), *2011 Materials Research Society (MRS) Fall Meeting*, Boston, Massachusetts, Nov.-Dec. 2011.
5. R. K. Juday, K. W. Sun, A. M. Fischer, F. A. Ponce, H. J. Kim, S. Choi, J. Kim, M.-H. Ji, J.-H. Ryou, and R. D. Dupuis, "Hydrogen-related cathodoluminescence in Mg-doped GaN" (Y10), *53rd Electronic Materials Conference (EMC 2011)*, Santa Barbara, California, Jun. 2011.
6. J. Kim, M.-H. Ji, S. Choi, J.-H. Ryou, R. D. Dupuis, K. W. Sun, R. K. Juday, A. M. Fischer, and F. A. Ponce, "Enhancement of hole transport and carrier distribution in InGaN/GaN multiple-quantum wells by controlling indium content of p-type layer in visible light-emitting diodes" (M6), *53rd Electronic Materials Conference (EMC 2011)*, Santa Barbara, California, Jun. 2011.
7. S. Choi, M.-H. Ji, J. Kim, H. J. Kim, J.-H. Ryou, P. D. Yoder, R. D. Dupuis, K. W. Sun, A. M. Fischer, and F. A. Ponce, "Effect of $In_xAl_{1-x}N$ electron blocking layer on quantum efficiency in visible light-emitting diodes grown by metalorganic chemical vapor deposition" (M3), *53rd Electronic Materials Conference (EMC 2011)*, Santa Barbara, California, Jun. 2011.
8. R. D. Dupuis, S. Choi, H. J. Kim, J. Kim, M.-H. Ji, J.-H. Ryou, P. D. Yoder, K. W. Sun, A. M. Fischer, R. K. Juday, and F. A. Ponce, "Improvement of efficiency droop by employing InAlN electron blocking layers in III-N visible LEDs grown by metalorganic chemical vapor deposition," *2011 European Materials Research Society (E-MRS) Spring Meeting*, Nice, France, May 2011.
9. R. D. Dupuis, S. Choi, J. Kim, H. J. Kim, M.-H. Ji, J.-H. Ryou, P. D. Yoder, K. W. Sun, A. M. Fischer, R. K. Juday, and F. A. Ponce, "Improvement of efficiency droop by employing InAlN electron blocking layers in III-N visible LEDs grown by metalorganic chemical vapor deposition" (7954-13), *SPIE Photonics West - Opto 2011*, San Francisco, California, Jan. 2011.
10. R. D. Dupuis, J.-H. Ryou, H. J. Kim, J. P. Liu, Z. Lochner, J. Kim, S. Choi, and S.-S. Kim, "Recent advances in the MOCVD growth of III-N light emitting diodes" (ME+SS-ThM1), *57th AVS International Symposium and Exhibition (AVS-57)*, Albuquerque, New Mexico, Oct. 2010.
11. S. Choi, H. J. Kim, J. Kim, J.-H. Ryou, P. D. Yoder, R. D. Dupuis, M.-H. Ji, K. W. Sun, A. M. Fischer, R. K. Juday, and F. A. Ponce, "Improvement of efficiency droop by employing InAlN electron blocking layers in visible light-emitting diodes grown by metalorganic chemical vapor deposition" (H1.3), *International Workshop on Nitride Semiconductors (IWN 2010)*, Tampa, Florida, Sep. 2010.
12. A. M. Fischer, K. W. Sun, R. Juday, F. A. Ponce, J.-H. Ryou, H. J. Kim, S. Choi, S.-S. Kim, and R. D. Dupuis, "Effect of growth temperature on the properties of InAlN layers for high efficiency green emitting diodes" (M5.40), *17th International Microcopy Congress (IMC-17)*, Rio de Janeiro, Brazil, Sep. 2010.

13. H. J. Kim, S. Choi, S.-S. Kim, J.-H. Ryou, P. D. Yoder, R. D. Dupuis, K. W. Sun, A. M. Fischer, R. K. Juday, and F. A. Ponce, "Effect of InAlN electron blocking layer in visible light-emitting diodes on quantum efficiency grown by metalorganic chemical vapor deposition" (S1), *52nd Electronic Materials Conference (EMC 2010)*, Notre Dame, Indiana, Jun. 2010.
14. H. J. Kim, S. Choi, S.-S. Kim, J.-H. Ryou, P. D. Yoder, R. D. Dupuis, K. W. Sun, A. Fischer, and F. Ponce, "InAlN electron blocking layer in visible light-emitting diodes grown by metalorganic chemical vapor deposition," *15th International Conference of Metalorganic Vapor Phase Epitaxy (ICMOVPE XV)*, Incline Village, Nevada, May 2010.
15. J. H. Ryou, R. D. Dupuis, F. A. Ponce, S. Choi, J. Kim, Z. Lochner, J. Liu, H. J. Kim, A. M. Fisher, Z. Wu, and K. Sun, "Fundamental studies and development of III-N visible LEDs for high-power solid-state lighting applications," *2010 DOE Solid-State Lighting R&D Workshop*, Raleigh, North Carolina, Feb. 2010.
16. J.-W. Jeon, and T.-Y. Seong, H. Kim, J.-H. Ryou, and R. D. Dupuis, "Electrical characteristics of Ti/Al contacts to N-polar n-type GaN fro vertical LEDs" (NN10), *51st Electronic Materials Conference (EMC 2009)*, State College, Pennsylvania, Jun. 2009.
17. Z. Lochner, J. P. Liu, J.-H. Ryou, P. D. Yoder, and R. D. Dupuis, "Barrier effect on hole transport and carrier distribution in InGaN/GaN multiple quantum well visible light-emitting diodes" (LL2), *51st Electronic Materials Conference (EMC 2009)*, State College, Pennsylvania, Jun. 2009.
18. Z. Lochner, J. Liu, H. Kim, J. H. Ryou, R. D. Dupuis, A. M. Fisher, Z. Wu, K. Sun, and F. A. Ponce, "Fundamental studies and development of III-N visible LEDs for high-power solid-state lighting applications," *2009 DOE Solid-State Lighting R&D Workshop*, San Francisco, California, Feb. 2009.
19. R. D. Dupuis, J.-H. Ryou, J. Liu, and Z. Lochner, "High-brightness green light-emitting diodes for solid state lighting applications," *5th China International Forum & Exhibition on Solid State Lighting (CHINA SSL 2008)*, Shenzhen, China, Jul. 2008.
20. J. P. Liu, J.-H. Ryou, Z. Lochner, C. A. Horne, J. Limb, D. Yoo, R. D. Dupuis, Z. H. Wu, A. M. Fischer, and F. A. Ponce, "Visible LEDs grown on c-plane and a-plane free-standing substrates" (BB1), *50th Electronic Materials Conference (EMC 2008)*, Santa Barbara, California, Jun. 2008.
21. J. P. Liu, J.-H. Ryou, Z. Lochner, C. A. Horne, J. Limb, D. Yoo, and R. D. Dupuis, "Visible LEDs grown on c-plane and a-plane free-standing substrates" (F5), *7th International Symposium on Semiconductor Light Emitting Devices (ISSLED 2008)*, Phoenix, Arizona, Apr. 2008.

## *REFERENCES*

[1] M. G. Craford, "LEDs challenge the incandescents," *IEEE Circuits and Devices Magazine* **8**, Sep., 24-29 (1992).

[2] D. A. Steigerwald, J. C. Bhat, D. Collins, R. M Fletcher, M. O. Holcomb, M. J. Ludowise, P. S. Martin, and S. L. Ludaz, "Illumination with solid sate lighting technology," *IEEE J. Select. Topic. Quantum Electron.* **8**, 310-320 (2002).

[3] M. Peter, A. Laubsch, P. Stauss, A. Walter, J. Baur, and B. Hahn, *Phys. Stat. Sol. (c)* **5**, 2050 (2008).

[4] "*The Promise of Solid State Lighting for General Illumination—2002 Update*," DoE BTS and OIDA (Published by OIDA, Washington DC, 2002).

[5] M. R. Krames, O. B. Shchekin, R. Mueller-Mach, G. O. Mueller, L. Zhou, G. Harbers, and M. G. Craford, *J. Display Technol.* **3**, 160 (2007).

[6] T. Mukai, M. Yamada, and S. Nakamura, *Jpn. J. Appl. Phys.* **38**, 3976 (1999).

[7] F. A. Ponce, S. Srinivasan, A. Bell, L. Geng, R. Liu, M. Stevens, J. Cai, H. Omiya, H. Marui, and S. Tanaka, "Microstructure and electronic properties of InGaN alloys," *Phys. Stat. Sol. (b)* **240**, 273 (2003).

[8] A. A. Efremov, N. I. Bochkareva, R. I. Gorbunov, D. A. Lavrinovich, Yu. T. Rebane, D. V. Tarkhin, and Yu. G. Shreter, "Effect of the Joule heating on the quantum efficiency and choice of thermal condition for high-power blue InGaN/GaN LEDs, *Semiconductors* **40**, 605(2006).

[9] R. F. Kalricek, Liminus Devices Inc., Billerica, MA, private communication, 2007.

[10] T. Mukai, M. Yamada, and S. Nakamura, "Characteristics of InGaN-based UV/blue/green/amber/red light-emitting diodes," *Jpn. J. Appl. Phys.* **38**, 3976 (1999).

[11] A. Y. Kim, W. Gotz, D. A. Steigerwald, J. J. Wierer, N. F. Gardener, J. Sun, S. A. Stockman, P. S. Martin, M. R. Krames, R. S. Kern, and F. M. Steranka, "Performance of high-power AlInGaN light emitting diodes," *Phys. Stat. Sol. (a)* **188**, 15 (2001).

[12] K. Akita, T. Kyono, Y. Yoshizumi, H. Kitabayashi, and K. Katayama, "Improvements of external quantum efficiency of InGaN-based blue light-emitting diodes at high current density using GaN substrates," *J. Appl. Phys.* **101**, 033104 (2007).

[13] I. V. Rozhansky and D. A. Zakheim, "Analysis of processes limiting quantum efficiency of AlGaInN LEDs at high pumping," *Phys. Stat. Sol. (a)* **204**, 227 (2007).

[14] M. Kim, M. Schubert, Q. Dai, J. Kim, E. Schubert, J. Piprek, and Y. Park, "Origin of efficiency droop in GaN-based light-emitting diodes," *Appl. Phys. Lett.* **91**, 183507 (2007).

[15] J. P. Liu, J.-H. Ryou, R. D. Dupuis, J. Han, G. D. Shen, and H. B. Wang, "Barrier effect on hole transport and carrier distribution in InGaN/GaN multiple quantum well visible light-emitting diodes," *Appl. Phys. Lett.* **93**, 021102 (2008).

[16] X. Ni, Q. Fan, R. Shimada, U. Ozgur, and H. Morkoc, "Reduction of efficiency droop in InGaN light emitting diodes by coupled quantum wells," *Appl. Phys. Lett.* **93**, 171113 (2008).

[17] Y. C. Shen, G. O. Mueller, S. Watanabe, N. F. Gardner, A. Munkholm, and M. R. Krames, "Auger recombination in InGaN measured by photoluminescence," *Appl. Phys. Lett.* **91**, 141101 (2007).

[18] N. F. Gardner, G. O. Muller, Y. C. Shen, G. Chen, S. Watanabe, W. Gotz, and M. R. Krames, "Blue-emitting InGaN–GaN double-heterostructure light-emitting diodes reaching maximum quantum efficiency above 200 A/cm$^2$," *Appl. Phys. Lett.* **91**, 243506 (2007).

[19] K. T. Delaney, P. Rinke, and C. G. Van de Walle, "Auger recombination rates in nitrides from first principles," *Appl. Phys. Lett.* **94**, 191109 (2009).

[20] M. R. Krames, O. B. Shchekin, R. Muller-Mach, G. O. Muller, L. Zhou, G. Harbers and M. G. Craford, "Status and future of high-power light-emitting diodes for solid-state lighting," *J. Display Tech.* **3**, 160 (2007).

[21] J. B. Limb, W. Lee, J. H. Ryou, D. Yoo, and R. D. Dupuis, "Comparison of GaN and $In_{0.04}Ga_{0.96}N$ p-layers on the electrical and electroluminescence properties of green light emitting diodes," *J. Electron. Mater.* **36**, 426 (2007).

[22] W. Lee, J. Limb, J.-H. Ryou, D. Yoo, M. A. Ewing, Y. Korenblit, and R. D. Dupuis, "Nitride-based green light-emitting diodes with various p-type layers," *J. Display Technol.* **3**, 126 (2007).

[23] J. P. Liu, J. Limb, J.-H. Ryou, D. Yoo, C. A. Horne, and R. D. Dupuis, "Characteristics of green light-emitting diodes using InGaN:Mg/GaN:Mg superlattice as p-type hole injection and contact layers," *J. Electron. Mater.* **37**, 558 (2008).

[24] J.-H. Ryou, W. Lee, D. Yoo, J. B. Limb, R. D. Dupuis, Z. H. Wu, A. M. Fischer, and F. A. Ponce, "Control of quantum-confined Stark effect in InGaN/GaN multiple quantum well active region by p-type layer for III-nitride-based visible light-emitting diodes," *Appl. Phys. Lett.* **92**, 101113 (2008).

[25] J. P. Liu, J. Limb, Z. Lochner, D. Yoo, J.-H. Ryou, and R. D. Dupuis, "Green light-emitting diodes with p-InGaN:Mg grown on c-plane sapphire and GaN substrates," *Phys. Stat. Sol (a)* **206**, 750 (2009).

[26] X. A. Cao, S. F. LeBoeuf, M. P. D'Evelyn, S. D. Arthur, J. Kretchmer, C. H. Yan, and Z. H. Yang, "Blue and near-ultraviolet light-emitting diodes on free-standing GaN substrates," *Appl. Phys. Lett.* **84**, 4313-4315 (2004).

[27] T. Kyono, H. Hirayama, K. Akita, T. Nakamura, and K. Ishibashi, "Effects of In composition on ultraviolet emission efficiency in quaternary InAlGaN light-emitting diodes on freestanding GaN substrates and sapphire substrates," *J. Appl. Phys. Lett.* **98**, 113514-1-8 (2005).

[28] S. Choi, H. J. Kim, J.-H. Ryou, and R. D. Dupuis, "Actual temperatures of growing surfaces of III-nitride-based materials depending on substrates and forced convection conditions in metalorganic chemical vapor deposition," *J. Appl. Phys.* **106**, 073512-1-6 (2009).

[29] H. Chen, R. M. Feenstra, J. E. Northrup, T. Zywietz, and J. Neugebauer, "Spontaneous formation of indium-rich nanostructures on InGaN (0001) surfaces," *Phys. Rev. Lett.* **85**, 1902-1905 (2000).

[30] I.-K. Park, M.-K. Kwon, S.-H. Baek, Y.-W. Ok, T.-Y. Seong, S.-J. Park, Y.-S. Kim, Y.-T. Moon, and D.-J. Kim, "Enhancement of phase separation in the InGaN layer for self-assembled In-rich quantum dots," *Appl. Phys. Lett.* **87**, 061906-1-3 (2005).

[31] M. Maier, K. Köhler, M. Kunzer, W. Pletschen, and J. Wagner, "Reduced nonthermal rollover of wide-well GaInN light-emitting diodes," *Appl. Phys. Lett.* **94**, 041103-1-3 (2009).

[32] J. P. Liu, J. Limb, J.-H. Ryou, D. Yoo, C. A. Horne, R. D. Dupuis, Z. H. Wu, A. Fischer, F. A. Ponce, A. D. Hanser, L. Liu, E. A. Preble, and K. R. Evans "Blue light emitting diodes grown on free standing (1 1-20) a-plane GaN substrates," *Appl. Phys. Lett.* **92**, 011123 (2008).

[33] J.-H. Ryou, J. Limb, W. Lee, J. Liu, Z. Lochner, D. Yoo, and R. D. Dupuis, "Effect of silicon doping in the quantum-well barriers on the electrical and optical properties of visible green light-emitting diodes," *IEEE Photon. Tech. Lett.* **20**, 1769 (2008).

[34] J.-H. Ryou, P. D. Yoder, J. P. Liu, Z. Lochner, H. Kim, S. Choi, and H. J. Kim, and R. D. Dupuis, "Control of quantum confined Stark effect in InGaN-based quantum wells," *IEEE J. Select. Topic. Quantum Electron.* **15**, 1080 (2009).

[35] H. J. Kim, S. Choi, S.-S. Kim, J.-H. Ryou, P. D. Yoder, R. D. Dupuis, A. M. Fischer, and F. A. Ponce, "Improvement of quantum efficiency by employing active-layer-friendly lattice-matched InAlN electron blocking layer in green light-emitting diodes," *Appl. Phys. Lett.* **96**, 101102 (2010).

[36] A. M. Fischer, K. W. Sun, R. Juday, F. A. Ponce, J.-H. Ryou, H. J. Kim, S. Choi, S.-S. Kim, and R. D. Dupuis, "Effect of growth temperature on the electron-blocking performance of InAlN layers in green emitting diodes," *Appl. Phys. Exp.* **3**, 031003 (2010).

[37] S. Choi, H. J. Kim, S.-S. Kim, J. P. Liu, J. Kim, J.-H. Ryou, R. D. Dupuis, A. M. Fischer, and F. A. Ponce, "Improvement of peak quantum efficiency and efficiency droop in III-nitride visible light-emitting diodes with an InAlN electron blocking layer," *Appl. Phys. Lett.* **96**, 221105 (2010).

[38] J. Kim, M.-H. Ji, Z. Lochner, S. Choi, J. P. Liu, Md. M. Satter, P. D. Yoder, J.-H. Ryou, R. D. Dupuis, R. Juday, A. M. Fischer, and F. A. Ponce, "Role of p-$In_xGa_{1-x}N$ layer in enhancing hole transport and distribution in InGaN/GaN multiple quantum wells of visible III-nitride light-emitting diodes," *Appl. Phys. Exp.* (submitted for publication).

[39] S. Choi, M.-H. Ji, J. Kim, H. J. Kim, Md. M. Satter, J.-H. Ryou, P. D. Yoder, R. D. Dupuis, A. M. Fischer, and F. A. Ponce, "Efficiency droop due to electron spill-over and limited hole transport in III-nitride visible light-emitting diodes employing lattice-matched InAlN electron blocking layers," *Appl. Phys. Lett.* (submitted for publication).

[40] T. Li, Q. Y. Wei, A. M. Fischer, Y. Huang, F. A. Ponce, J. P. Liu, Z. Lochner, J.-H. Ryou, and R. D. Dupuis, "The effect of InGaN underlayers on the electronic and optical properties of blue-emitting InGaN/GaN quantum wells," *Appl. Phys. Lett.* (to be submitted for publication).